

Optical excitations in organic molecules, clusters and defects studied by first-principles Green's function methods

Murilo L. Tiago^(a) and James R. Chelikowsky^(a,b)

^(a) Center for Computational Materials, Institute for Computational Engineering and Sciences, University of Texas, Austin, TX 78712, USA.

^(b) Departments of Physics and Chemical Engineering, University of Texas, Austin, TX 78712, USA.
(Dated: April 15, 2024)

Spectroscopic and optical properties of nanosystems and point defects are discussed within the framework of Green's function methods. We use an approach based on evaluating the self-energy in the so-called GW approximation and solving the Bethe-Salpeter equation in the space of single-particle transitions. Plasmon-pole models or numerical energy integration, which have been used in most of the previous GW calculations, are not used. Fourier transforms of the dielectric function are also avoided. This approach is applied to benzene, naphthalene, passivated silicon clusters (containing more than one hundred atoms), and the F center in LiCl. In the latter, excitonic effects and the $1s\ 2p$ defect line are identified in the energy-resolved dielectric function. We also compare optical spectra obtained by solving the Bethe-Salpeter equation and by using time-dependent density functional theory in the local, adiabatic approximation. From this comparison, we conclude that both methods give similar predictions for optical excitations in benzene and naphthalene, but they differ in the spectra of small silicon clusters. As cluster size increases, both methods predict very low cross section for photoabsorption in the optical and near ultra-violet ranges. For the larger clusters, the computed cross section shows a slow increase as function of photon frequency. Ionization potentials and electron affinities of molecules and clusters are also calculated.

I. INTRODUCTION

Universality and predictive power are characteristic features of good first-principles theories. Such theories are invaluable as guides for experimental work, especially when knowledge about the system being investigated is limited. Density-functional theory (DFT) is recognized as state-of-the-art theory for the calculation of various ground-state properties of electronic systems from first principles, having been applied to a variety of different systems ranging from crystalline semiconductors to surfaces and nanostructures¹. In contrast, DFT has known difficulties in predicting quantities associated with excited states, which is not surprising since it was first proposed as a ground-state theory. As an example, the electronic band structure provided by DFT consistently shows an underestimated gap between valence and conduction bands^{1,2,3,4}. As consequence, the electronic band structure provided by DFT gives poor predictions for the onset of photoemission and inverse photoemission^{2,4}. Exact-exchange functionals improve results considerably for molecular systems⁵, but more work is needed in crystalline systems⁶. Gap narrowing also affects the linear optical spectrum, when calculated from single-electron transitions from the valence band to the conduction band^{4,7}.

Spectroscopic and optical properties of semiconductors have been successfully predicted from ab initio Green's function methods^{4,7}. The GW approximation has been used to provide the quasiparticle band structure of semiconductors, large-gap insulators, metals, surfaces, nanostructures and other materials⁴. By solving the Bethe-Salpeter equation for electrons and holes, the linear optical spectrum can also be obtained, providing reliable

results for the optical gap and excitonic effects^{7,8,9,10,11}. Since knowledge of the electron self-energy is required in solving the Bethe-Salpeter equation (BSE), this method is often referred to as GW + BSE¹². Although powerful, the GW + BSE method is very complex when applied to non-periodic systems, especially when discrete Fourier analysis is not applicable and approximations such as the generalized plasmon pole model² do not lead to substantial simplification. Some materials that fall in this category are confined systems: quantum dots, clusters, molecules, nanostructures. On the other hand, nanostructures are now the subject of intense work due to promising technological applications and recent advances in the preparation of artificial nanostructures^{13,14}. At the same time, significant effort has been dedicated on the theory side. Some of the difficulties one may encounter by applying the GW approximation to large molecules were emphasized recently^{15,16}. So far, reliable calculations of electronic self-energy within the GW approximation have been done for confined systems with up to a few tens of atoms^{8,9,17,18,19}. Similarly, the Bethe-Salpeter equation has been solved for a limited number of confined systems. During the last decade, optical properties of confined systems have been investigated within time-dependent DFT, often with very good results^{7,20}. Time-dependent density DFT in the local, adiabatic approximation (TD-LDA) is formally simpler than the GW + BSE theory, but at the same time directed towards solving the same problem: predicting optical properties and neutral excitations in an electronic system. A drawback of TD-LDA is that it reportedly fails to predict correct optical gaps and excitonic effects in extended systems^{7,21}. Alternative TDDFT functionals which include many-body effects have been proposed^{21,22,23,24,25}.

As mathematical simplification, applications of the GW + BSE method in nanostructures frequently impose artificial periodicity by placing the electronic system in a large supercell¹⁷. This is a perfectly justifiable procedure, but it has the obvious deficiency of increasing the computational effort when supercells are required to be large. A more efficient procedure would be to take advantage of properties intrinsic to confined systems and design a numerical implementation of such Green's function methods, and we now propose one such implementation. A key ingredient is electronic screening. We incorporate it into the theory by computing the electron polarizability function in two approximations: random-phase approximation (RPA) and TD-LDA. The electron self-energy is calculated from first principles and the Bethe-Salpeter equation is set and solved in the space of single-particle transitions. In this framework, many-body functions are expressed as matrices in this transition space and in energy (frequency) representation. Fourier transforms are not needed, and energy integrations are evaluated by integrations over poles. Portions of this work have been reported earlier²⁶.

The methodology proposed here is applied to a number of interesting cases. One of them is isolated oligoacenes, for which extensive experimental data is available but the only GW-based analysis known to us have been published recently¹⁵. The second application is in silicon nanoclusters, studied previously within TD-LDA²⁰ and, for the smaller clusters, GW + BSE^{8,18}. Here, we investigate clusters with bulk-like crystalline structure and report benchmark GW + BSE calculations for clusters with more than one hundred silicon atoms. The last application is in the F-center defect in LiCl. This is a challenging case, with characteristics of both confined and periodic system. We show that the resulting optical spectrum correctly contains both the signature of defect levels located within the band gap and electron-hole interactions. The latter manifest themselves in the energy-resolved dielectric function as an exciton feature below the electronic band gap. TD-LDA is shown to predict an optical transition between two defect levels, but the exciton feature is not found. The paper is organized as follows: in Section II, we present the theoretical framework, starting from TD-LDA and continuing through the GW method and solution of the Bethe-Salpeter equation. Section III is devoted to applications, containing one subsection for each particular system: oligoacenes, silicon clusters, and F-center in LiCl. We draw final conclusions in Section IV.

II. THEORY

A. Linear response within TD-LDA

Gross and Kohn²⁷ have shown how to extend DFT to the time-dependent case by analyzing the effect on the charge density upon the action of an external potential that changes in time. Their theoretical approach can be further simplified by making use of two assumptions^{7,20,28}: adiabatic limit, and local-density approximation, under which the exchange-correlation kernel is instantaneous in time and a sole function of charge density at each point in space. This is the time-dependent local-density approximation (TD-LDA)^{20,28,29,30}.

When the external potential is due to an applied electric field, the linear response in charge density is related to the external potential via a response function (the polarizability) according to

$$\epsilon_f(1;2) = \frac{\langle 1 \rangle}{V_{\text{ext}}(2)} ; \quad (1)$$

where we use a many-body notation for space-time and spin variables: $\langle 1 \rangle = \langle r_1; t_1; \uparrow \rangle$. The subscript f indicates that the response function above is calculated within TD-LDA. Working in frequency domain²⁸, the TD-LDA polarizability can be written as a sum over normal modes,

$$\epsilon_f(r; r^0; E) = \frac{2}{h} \sum_s \frac{\langle s(r) | s(r^0) \rangle}{E - \epsilon_s + i0^+} ; \quad (2)$$

where the normal modes of excitation in the system are denoted by ϵ_s , and 0^+ represents a positive infinitesimal²³. We assume $\hbar = 1$ throughout. The factor of 2 comes from summation over spin indices. Still following the frequency-domain formulation by Casida^{20,28}, the amplitudes $\langle s(r) |$ are obtained by solving a generalized eigenvalue problem. In order to obtain the desired eigenvalue equation, we first expand $\langle s$ in a series of single-particle transitions from an occupied level v to an unoccupied level c :

$$\langle s(r) | = \sum_{vc} X_{vc}^s \langle v(r) | \langle c | ; \quad (3)$$

where Kohn-Sham eigenvalues are denoted ϵ_i , with corresponding eigenfunctions $\langle i |$. For clarity, we reserve indices v, v^0 for occupied orbitals and indices c, c^0 for unoccupied orbitals. The coefficients X above satisfy an eigenvalue equation in $(\epsilon^2)^{28}$:

$$R^{1=2} R + 4(K^X + K^{\text{LDA}}) R^{1=2} X = \epsilon_s^2 X ; \quad (4)$$

in silicon clusters from first principles³⁴. The importance of Eq. (12) is that it provides a direct relationship between polarizability and inverse dielectric function. For completeness, we present expressions for the dielectric function and its inverse within the RPA :

$$\chi_0^{-1}(r; r^0; E) = \chi_0(r; r^0) + \int dr^{\text{int}} V(r; r^{\text{int}}) \chi_0(r^{\text{int}}; r^0; E) ; \quad (15)$$

$$\chi_0(r; r^0; E) = \chi_0(r; r^0) - \int dr^{\text{int}} V(r; r^{\text{int}}) \chi_0(r^{\text{int}}; r^0; E) ; \quad (16)$$

where χ_0 is the RPA polarizability, evaluated from Eqs. (2), (3) and (4) after setting $f_{xc} = 0$.

B. Electronic self-energy

A key quantity in solving the Bethe-Salpeter equation for optical excitations is the electronic self-energy, which can be computed from first principles within the GW approximation (GWA)^{2,3,4}. The basis of this approximation lies in the so-called "Hedin equations", a set of non-linear many-body equations which relate the self-energy with Green's function G , polarizability, screened Coulomb potential W , and vertex function³:

$$W(1;2) = V(1;2) + \int d(3) V(1;3) \chi_0(3;4) W(4;2) ; \quad (17)$$

$$\Sigma(1;2) = i \int d(3) G(1;3) G(4;1^+) \chi_0(3;4;2) ; \quad (18)$$

$$\Gamma(1;2) = i \int d(3) G(1;3) W(4;1^+) \chi_0(3;2;4) ; \quad (19)$$

$$\begin{aligned} \Sigma(1;2;3) &= \Sigma(1;2) \chi_0(1;3) \\ &+ \int d(4,5,6,7) \frac{\chi_0(1;2)}{G(4;5)} G(4;6) G(7;5) \chi_0(6;7;3) \end{aligned} \quad (20)$$

The approach taken by Hedin essentially generates a perturbation series in the screened interaction W . This expansion is expected to converge faster than an expansion in powers of the bare Coulomb potential V , as long as electronic screening is strong. Following this assumption³, the self-energy in Eq. (20) is first taken as zero and the vertex function reduces then to a delta function:

$$\Gamma(1;2;3) = \chi_0(1;2) \chi_0(1;3) ;$$

With that vertex function, the polarizability reduces to the RPA³:

$$\chi_0(1;2) = \chi_0(1;2) + \int d(3) V(1;3) \chi_0(3;2) ;$$

The screened Coulomb interaction is evaluated in terms of the dielectric function. From Eq. (17), one gets:

$$\begin{aligned} W_0(1;2) &= V(1;2) + \int d(3) V(1;3) \chi_0(3;2) ; \\ &= V(1;2) + \int d(3) \chi_0^{-1}(1;3) V(3;2) \\ &= V(1;2) + \int d(3) V(1;3) \chi_0(3;4) V(4;2) ; \end{aligned}$$

and the self-energy is

$$\Sigma(1;2) = iG(1;2)W_0(2;1^+) ; \quad (21)$$

The first ab initio calculations of self-energies for semiconductors^{2,35} followed the method outlined above. For periodic systems, the dielectric function can be conveniently expanded in plane wave basis and numerically inverted. Matrix inversion is a reasonably inexpensive step when the plane-wave expansion has a few hundreds or thousands of components. Dynamical effects can be included for instance by inverting the dielectric function at some values of frequency and either performing numerical integration over the frequency axis^{4,35}, or using a generalized plasmon pole model².

On the other hand, numerical inversion of the dielectric matrix in real space is problematic because of the size of the matrix. As an example, a converged calculation for the ground state of the silane molecule (SiH₄) requires a real-space grid containing about 10⁵ points³⁴. Inverting the dielectric function in real space would require inverting a dense matrix of size 10⁵ × 10⁵. Although straightforward, this task requires an extremely large amount of floating point operations and CPU memory. This is certainly an extreme situation, but it illustrates the type of problems involved with straight matrix inversion. The same issue is present in periodic systems with large periodic cells: since the number of plane-wave components in a Fourier expansion is proportional to the volume of the cell, direct matrix inversion of ϵ is also numerically expensive.

Significant numerical simplification is achieved by working in the representation of single-electron transitions³⁶, instead of using plane-wave or real-space representations for the dielectric function. There are two major advantages in doing that: the space of transitions is often much smaller than either the real space or reciprocal space, leading to matrices of reduced size; and integrations over frequency can be performed analytically since the polarizabilities χ_0 and χ_0 have known pole structure. In the space of transitions, a matrix element of the self-energy between Kohn-Sham orbitals j and j^0 is given schematically by:

$$\text{hjj}(\mathbb{E}^0)\text{jj}^0\text{i} = \text{hjj} \int_{\mathbb{Z}} \frac{d\mathbb{E}}{2} e^{i\mathbb{E}^0+} G(\mathbb{E}^0 - \mathbb{E}) [V + V_0(\mathbb{E})V] \text{jj}^0\text{i} : \quad (22)$$

The integral above can be replaced with a sum over poles below the real energy axis. Following Hedin^{3,37}, we write it as a summation of two terms: a bare exchange contribution χ and a correlation contribution c ,

$$\text{hjj}_x \text{jj}^0\text{i} = \sum_n^{\text{occ}} K_{njn}^x \text{jj}^0\text{i} ; \quad (23)$$

$$\text{hjj}_c(\mathbb{E}) \text{jj}^0\text{i} = 2 \sum_n^{\text{X}} \sum_s^{\text{X}} \frac{V_{nj}^s V_{n'j'}^s}{E - \epsilon_n - \epsilon_{s n}} ; \quad (24)$$

where

$$V_{nj}^s = \sum_{vc} K_{njvc}^x \frac{\epsilon_c - \epsilon_v}{\epsilon_s} \sum_{vc}^s : \quad (25)$$

The derivation of Eqs. (23), (24) and (25) from Eq. (22) is outlined in Appendix A. Whereas the summation over n in Eq. (23) is performed over all occupied Kohn-Sham orbitals, Eq. (24) has a summation over occupied and unoccupied orbitals. One can accelerate convergence in the last summation by truncating it and evaluating the remainder under the static approximation (see Appendix B). The coefficient ϵ_n has value +1 for unoccupied orbitals and -1 for occupied orbitals. In the equations above, eigenvectors X and eigenvalues ϵ are still evaluated under the random-phase approximation, obtained by setting $f_{xc} = 0$ in Eq. (4). In the following discussion, we refer to this level of approximation for the self-energy as GW_0 .

At this point, it is natural to advance one step further and use dielectric screening within TDLDA instead of RPA. The impact of TDLDA screening in the context of the GW approximation in bulk silicon has been analyzed before^{2,24,38}. In order to have a controlled level of approximation in Hedin's equations, we return to Eq. (20) and start an iterative solution by assuming $\text{hjj}(\mathbb{E}) V_{xc}(\mathbb{E}) \text{jj}^0\text{i} = \text{hjj}(\mathbb{E}) V_{xc}(\mathbb{E}) \text{jj}^0\text{i}$. The vertex function then becomes

$$\text{hjj}(\mathbb{E}) V_{xc}(\mathbb{E}) \text{jj}^0\text{i} = \text{hjj}(\mathbb{E}) V_{xc}(\mathbb{E}) \text{jj}^0\text{i} + \int_{\mathbb{Z}} d\mathbb{E}' \text{hjj}(\mathbb{E}) V_{xc}(\mathbb{E}) G(\mathbb{E} - \mathbb{E}') V_{xc}(\mathbb{E}') \text{jj}^0\text{i} : \quad (26)$$

The irreducible polarizability is now

$$\text{hjj}(\mathbb{E}) V_{xc}(\mathbb{E}) \text{jj}^0\text{i} = \text{hjj}(\mathbb{E}) V_{xc}(\mathbb{E}) \text{jj}^0\text{i} + \int_{\mathbb{Z}} d\mathbb{E}' \text{hjj}(\mathbb{E}) V_{xc}(\mathbb{E}) G(\mathbb{E} - \mathbb{E}') V_{xc}(\mathbb{E}') \text{jj}^0\text{i} : \quad (27)$$

For the screened Coulomb interaction, we write Eq. (17) in terms of the full polarizability operator:

$$\text{hjj}(\mathbb{E}) V_{xc}(\mathbb{E}) \text{jj}^0\text{i} = \text{hjj}(\mathbb{E}) V_{xc}(\mathbb{E}) \text{jj}^0\text{i} + \int_{\mathbb{Z}} d\mathbb{E}' \text{hjj}(\mathbb{E}) V_{xc}(\mathbb{E}) G(\mathbb{E} - \mathbb{E}') V_{xc}(\mathbb{E}') \text{jj}^0\text{i} ;$$

with

$$\text{hjj}(\mathbb{E}) V_{xc}(\mathbb{E}) \text{jj}^0\text{i} = \text{hjj}(\mathbb{E}) V_{xc}(\mathbb{E}) \text{jj}^0\text{i} + \int_{\mathbb{Z}} d\mathbb{E}' \text{hjj}(\mathbb{E}) V_{xc}(\mathbb{E}) G(\mathbb{E} - \mathbb{E}') V_{xc}(\mathbb{E}') \text{jj}^0\text{i} :$$

From Eq. (27), we get

$$\text{hjj}(\mathbb{E}) V_{xc}(\mathbb{E}) \text{jj}^0\text{i} = \text{hjj}(\mathbb{E}) V_{xc}(\mathbb{E}) \text{jj}^0\text{i} + \int_{\mathbb{Z}} d\mathbb{E}' \text{hjj}(\mathbb{E}) V_{xc}(\mathbb{E}) G(\mathbb{E} - \mathbb{E}') V_{xc}(\mathbb{E}') \text{jj}^0\text{i} + f_{xc}(\mathbb{E}) \text{hjj}(\mathbb{E}) V_{xc}(\mathbb{E}) \text{jj}^0\text{i} : \quad (28)$$

Although written in real-space representation, the function above is identical to Eq. (2), and we refer to it as χ in the subsequent discussion. This function describes polarization due to an external potential accompanied by dynamical screening produced by the self-consistent field. Finally, we arrive at the following expression for the self-energy:

$$\text{hjj}(\mathbb{E}) V_{xc}(\mathbb{E}) \text{jj}^0\text{i} = iG(\mathbb{E}) V_{xc}(\mathbb{E}) \text{jj}^0\text{i} + \int_{\mathbb{Z}} d\mathbb{E}' \text{hjj}(\mathbb{E}) V_{xc}(\mathbb{E}) G(\mathbb{E} - \mathbb{E}') V_{xc}(\mathbb{E}') \text{jj}^0\text{i} + f_{xc}(\mathbb{E}) \text{hjj}(\mathbb{E}) V_{xc}(\mathbb{E}) \text{jj}^0\text{i} : \quad (28)$$

We note that the use of TDLDA screening in the self-energy causes the inclusion of a vertex term (the second term inside curly brackets above). This level of approximation has been used before in the study of the quasi-particle band structure of crystalline silicon³⁸. Eq. (28) is a valid approximation for the self-energy but it is not symmetric with respect to the interchange of indices 1 and 2. In principle, this symmetry is not present in Eq. (19), but it can be recovered by defining a "left-sided" vertex function written schematically as $\chi = iW G$ as opposed to $\chi = iG W$ (c.f. Eq. 19)³¹. This deficiency is corrected by symmetrizing the last term in Eq. (28). Schematically, we rewrite $\chi = iG [V + V_{\text{eff}} V + f_{\text{eff}} V]$ as $\chi = iG [V + V_{\text{eff}} V + \frac{1}{2} V_{\text{eff}} V + \frac{1}{2} f_{\text{eff}} V]$. Matrix elements of the self-energy are then given by:

$$\text{hjj}(\mathbb{E}^0)\text{jj}^0\text{i} = \text{hjj} \int_{\mathbb{Z}} \frac{d\mathbb{E}}{2} e^{i\mathbb{E}^0+} G(\mathbb{E}^0 - \mathbb{E}) [V + V_{\text{eff}}(\mathbb{E})V + \frac{1}{2} V_{\text{eff}}(\mathbb{E})V + \frac{1}{2} f_{\text{eff}}(\mathbb{E})V] \text{jj}^0\text{i} : \quad (29)$$

This self-energy operator is written as a sum of three

contributions: $\chi = \chi_x + \chi_c + \chi_f$, where the first two

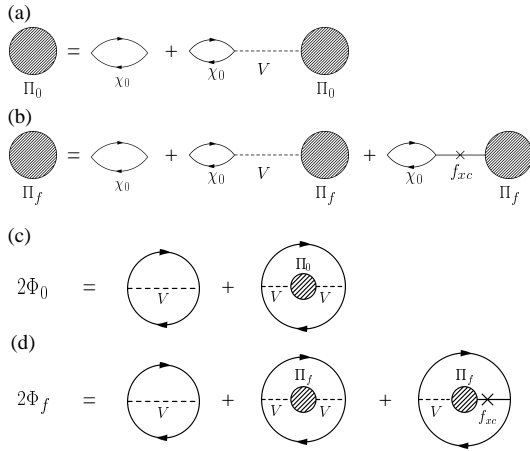


FIG. 1: Feynman diagrams for the polarizability operator (a,b) and the function (c,d). The local exchange-correlation kernel is represented by a crossed line. Solid oriented lines are Green's functions. Dashed lines denote the bare Coulomb potential.

terms are given by Eqs. (23) and (24) respectively, but now with full TD-LDA screening ($f_{xc} \neq 0$). The last term is a vertex correction:

$$h_{jj'}^s(E) \chi_{ij}^0 = \sum_n \sum_s \frac{V_{nj}^s F_{nj^0}^s + F_{nj}^s V_{nj^0}^s}{E - \epsilon_n^s}; \quad (30)$$

with

$$F_{nj}^s = \sum_{vc} K_{njvc}^{LDA} \frac{v_c}{\epsilon_s} \sum_{vc}^{l=2} X_{vc}^s; \quad (31)$$

In order to make distinction between the two levels of approximation, we refer to the last approximation (Eq. 29) as GW_f , as opposed to GW_0 , Eq. (22).

It is not unexpected that, by using a polarizability function from TD-LDA, we obtain a self-energy operator that has vertex corrections. In the language of many-body physics, the assumption in Eq. (26) implies that additional Feynman diagrams are included in the polarizability and in the self-energy. Fig. 1(a,b) shows the diagrams included in the polarizability for both RPA and TD-LDA. Although such diagrams include the LDA kernel, which does not have expansion in G and V , we can still define a many-body function such that $\chi(l;2) = G(l;2)$. The diagrams for χ are depicted in Fig. 1(c,d). Adding the last diagram in Fig. 1(b) amounts to enhanced screening, since it allows for a new channel for electrons to redistribute in the presence of an external potential. This is counterbalanced by the inclusion of a vertex diagram (right-most diagram in Fig. 1(d)). We also note that Fig. 1 provides a justification for symmetrizing Eq. (28): differentiating the additional vertex diagram with respect to G leads to a pair of diagrams consistent with Eq. (30).

Inclusion of self-energy corrections in the description of the electronic system is done following the usual procedure: we assume the quasiparticle approximation and write down an eigenvalue equation for quasiparticles^{2,4},

$$[H_{LDA} + V_{xc}] \psi_j = E_j \psi_j; \quad (32)$$

where quasiparticle orbitals ψ_j are expanded in the basis of Kohn-Sham eigenfunctions and H_{LDA} is the (diagonal) LDA Hamiltonian⁴. Quasiparticle energies and wave-functions are now found by direct diagonalization of the equation above.

In writing Eq. (32), we should consider carefully the energy dependence of V_{xc} . Hybertsen and Louie² have shown that evaluating the self-energy around the quasiparticle energy leads to accurate band structures for cubic semiconductors. Since the quasiparticle energy is not known before Eq. (32) is solved, the suggested procedure² is to evaluate the operator $h(E) = V_{xc} + \Sigma(E) - V_{xc}$ and its energy derivative at the LDA eigenvalue, $E = E_{LDA}$, and use linear extrapolation for the actual quasiparticle energy. We follow a similar methodology: first, we evaluate the diagonal part of the quasiparticle Hamiltonian in Eq. (32) and obtain a first estimate for quasiparticle energies by solving the equation $E_j = \epsilon_j + h_{jj}(E_j) - V_{xc}$. In the next step, we include off-diagonal matrix elements and proceed through full diagonalization. At the end, quasiparticle energies are still close to their first estimate.

An open issue regarding the GW method is whether self-consistency between self-energy, polarizability and Green's function should be imposed or not and, if so, how to do it³⁹. When the GW_0 and GW_f approximations were obtained by iterating Hedin's equations, self-consistency was lost and the vertex function was drastically simplified. Early work has indicated that self-consistency and vertex contributions partially cancel each other⁴⁰, which may explain the remarkable success of the GW method for semiconductors. There have been some attempts at imposing partial self-consistency between self-energy and Green's function^{2,4}, which resulted in quasiparticle energies improved by a fraction of electron-volt. Nevertheless, full self-consistency between self-energy and Green's function was observed to degrade the quasiparticle bandwidth and the description of the satellite structure in the electron gas⁴¹. In the subsequent applications, we do not attempt to impose self-consistency. Instead, the single-particle Green's function is always constructed from Kohn-Sham eigenvalues and eigenfunctions.

C. Bethe-Salpeter equation

While the GW method provides a description of quasiparticles in the system (i.e., the energy needed to add or extract one electron from the system), the solution of the Bethe-Salpeter equation gives information about neutral

excitations: the process of promoting electrons from occupied quasiparticle orbitals to unoccupied ones. The important Green's function now is no longer the one-electron Green's function but the two-particle or, more specifically, the electron-hole Green's function³¹.

We start with a many-body expression for the polarizability:

$$(1;2) = iL(1;2;1^+;2^+); \quad (33)$$

where L is the electron-hole correlation function^{7,8,31}, which satisfies the Bethe-Salpeter equation:

$$L(1;2;3;4) = G(1;4)G(2;3) + \int d(5678)G(1;5)G(6;3)K(5;7;6;8)L(8;2;7;4) \quad (34)$$

The kernel operator K describes interactions between the excited electron and the "hole" left behind in the electron sea. The connection with GW is present in two aspects:

1. The Green's function that enters in Eq. (34) is the Green's function for the interacting electronic system. Within the quasiparticle approximation, it is calculated with eigenvalues and wave-functions obtained by diagonalizing Eq. (32).
2. The kernel K is related to the self-energy by^{7,8,31}:

$$K(1;2;3;4) = i(1;3)(2;4)V(1;2) + \frac{(1;3)}{G(4;2)}; \quad (35)$$

Although the functions G and K can be evaluated in many approximations, it is important to retain the same level of approximation in both quantities, so that all important Feynman diagrams are included and no diagrams are double-counted. In the lowest level of approximation, many-body effects can be ignored completely and the self-energy approximated by the LDA exchange-correlation potential, $(1;2) = V_{xc}(1)(1;2)$. In this case, the Green's function to be used is constructed from LDA eigenvalues and eigenfunctions, and Eq. (34) reduces itself to the TD-LDA eigenvalue equation, Eq. (4). This fact has been explored in recent studies where model exchange-correlation functionals are designed to work as good approximations for the self-energy in Eq. (35) while retaining as much as possible the formal simplicity of TD-LDA^{7,21,23}. By its own nature, this family of approximations does not have Feynman diagrams in terms of which the self-energy is expanded.

Another level of approximation is GW_0 , Eq. (22). The kernel K has then two terms: a bare exchange interaction, originated from the first term in Eq. (35), and a screened interaction, from $\Sigma = G = iW_0$. This approximation has been used in a variety of different applications with very good results (see e.g.^{7,8}).

Finally, a third level of approximation is GW_f , Eq. (29). At this level, the kernel has an additional term besides the previous two: a LDA vertex correction. As opposed to the kernel present in the TD-LDA equation, the BSE kernel within either GW_0 or GW_f has explicit energy dependence, from the polarizability operator. This dependence was observed to be negligible when the interaction kernel itself is weak⁸. Ignoring dynamical effects and ignoring the mixing of absorption and emission contributions in the kernel^{9,4}, one can rewrite Eq. (34) as an eigenvalue equation^{7,8}:

$$iA_{vc}^1 = (E_c - E_v)A_{vc}^1 + \int_{v'c'}^P 2K_{vcv'c'}^x + K_{vcv'c'}^d + K_{vcv'c'}^f A_{v'c'}^1; \quad (36)$$

where $E_c; E_v$ are quasiparticle energies of unoccupied and occupied orbitals respectively. The exchange kernel K^x has the same form given by Eq. (6). The kernels K^d and K^f are given by:

$$K_{vcv'c'}^d = K_{vv'cc'}^x + 4 \sum_s \frac{V_{vv'}^s V_{cc'}^s}{i_s}; \quad (37)$$

$$K_{vcv'c'}^f = 2 \sum_s \frac{V_{vv'}^s F_{cc'}^s + F_{vv'}^s V_{cc'}^s}{i_s}; \quad (38)$$

The eigenvectors A are normalized in the usual way, and the polarizability is now given by

$$\chi_{BSE}(r; r^0; E) = \sum_1^X \frac{\psi_1(r) \psi_1(r^0)}{E - \epsilon_1 + i0^+} \frac{\psi_1(r) \psi_1(r^0)}{E + \epsilon_1 - i0^+}; \quad (39)$$

with

$$\psi_1(r) = \sum_{vc}^X \psi_{vc}(r) A_{vc}^s; \quad (40)$$

As in the TD-LDA, the solution of the Bethe-Salpeter equation provides the electrostatic susceptibility tensor and absorption cross section by equations analogous to (8), (9), (11), with the replacements $i_s \rightarrow i_1$ and $!_s \rightarrow !_1$.

D. Technical considerations

Working in the space of single-particle transitions has two clear advantages: it does not assume any particular boundary condition over electron wave-functions, being equally valid for confined as well as extended systems; and it often leads to matrices smaller than the corresponding ones in real-space or reciprocal-space representations. In addition, the necessary numerical tasks are simple: matrix algebra (diagonalizations and matrix

products), and evaluation of integrals of the type in Eqs. (6) and (7). We can also take advantage of existing point symmetries in the system at hand and divide the transition space into different group representations, resulting in block-diagonal matrices. This method can be readily extended to periodic systems by adding lattice periodicity as an additional symmetry operation. Each block is then associated to a particular k -point in the Brillouin zone. For large systems, the solution of Eqs. (4) and (36) may involve large matrices, but further simplification is obtained by restricting the transition space to low-energy transitions. In the calculation of the self-energy terms Σ_c and Σ_f , one can proceed through the sum over single-particle states by including the static remainder (see appendix B).

III. APPLICATIONS

In order to assess the reliability of the current implementation, we have employed it to study the excited-state properties of different classes of systems, both localized and extended. In all applications, we start from the electronic system in its ground state, as described within DFT. The exchange-correlation potential is used in the Ceperley-Alder form⁴³. With the use of norm-conserving pseudopotentials⁴⁴, we are able to remove core electrons from the problem, reducing considerably the numerical effort. In all applications, we use pseudopotentials constructed according to the Troullier-Martins prescription⁴⁴. We employ a real-space approach in the solution of the Kohn-Sham Equation⁴⁵. In this approach, wave-functions are expressed directly as functions of position. For a finite system, wave-functions are required to vanish outside a spherical boundary with adjustable radius. The volume inside this boundary is sampled by a homogeneous grid with fixed grid spacing h along the three Cartesian directions. Results are tested for convergence with respect to the grid spacing and the boundary radius. We explore point symmetries both in the solution of the Kohn-Sham equation and in the calculation of integrals in Eqs. (6) and (7). For the self-energy operator, we include the static remainder according to appendix B. We carefully test convergence with respect to the highest state explicitly included in the summation. Except when noted, we compute self-energies at the GW_f level. Numerical accuracy in self-energy matrix elements is 0.2 eV or better. Excited states of the electronic system are calculated without the inclusion of effects due to structural relaxation.

A. Benzene and naphthalene

Having a relatively small number of valence electrons makes the benzene molecule, C_6H_6 , a good test system for the theory just presented. In addition, benzene has been the subject of extensive experiments, probing vari-

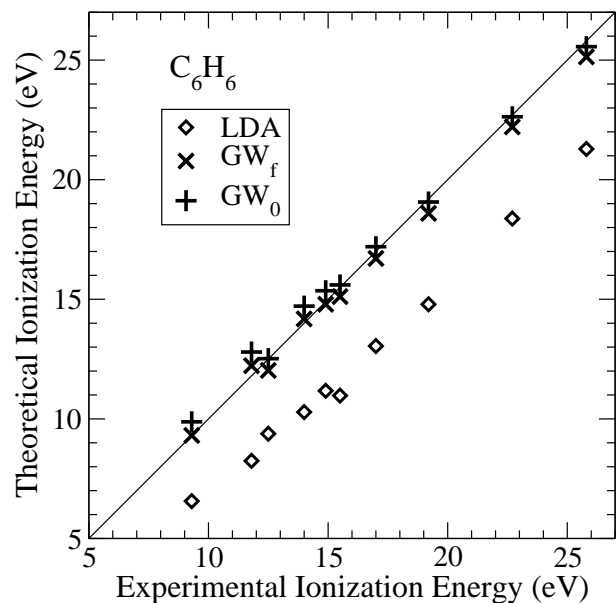


FIG. 2: Ionization energies of benzene, associated to all occupied orbitals in the molecule, as predicted within GW_0 and GW_f . The theoretical ionization energy is the negative of a quasiparticle energy eigenvalue. Experimental data from⁵⁴.

ous properties such as linear optical response, electronic structure and ionization⁴⁶. On the theory side, its optical properties have been investigated with both TD-LDA and GW -BSE approaches^{20,26,47}. Quasiparticle energy levels of benzene and other oligoacenes have also been recently calculated using a first-principles Gaussian orbital-based method as well as a tight-binding approach¹⁵. The series of oligoacenes, benzene being the first element, is a sequence of molecules composed of n co-joined aromatic rings, starting from $n = 1$ (benzene), $n = 2$ (naphthalene), etc. Oligoacene crystals have received renewed attention recently due to their potential use in organic thin film devices^{11,48}.

In our calculations, we solve the Kohn-Sham equations on a regular grid with grid spacing 0.4 a.u. (the Bohr radius being 1 a.u.). Electronic wave-functions were required to vanish outside a sphere of radius 16 a.u. centered on the molecule. Carbon-carbon and carbon-hydrogen bond lengths were fixed at their experimental values. The calculation of the self-energy operator was done including up to 305 unoccupied (virtual) orbitals in the TD-LDA polarizability and in the calculation of correlation and vertex parts. This ensures that the sum rule is satisfied to within 30%, which was found to be sufficient for an accuracy of 0.1 eV in quasiparticle energies. After the self-energy operator was computed, quasiparticle energies for occupied and unoccupied orbitals were obtained by diagonalizing the Hamiltonian in Eq. (32). Extensive convergence tests have been performed on all relevant numerical parameters: choices of 0.3 and 0.4 a.u. were used for the grid spacing; we have used boundary radii of up to 20 a.u., and included up to 1000 virtual

orbitals. For the last choice, the sum rule is satisfied to within 14%.

Fig. 2 shows a comparison between theoretical and experimental ionization energies. In the framework of the GW approximation, the first ionization energy is interpreted as the negative of the quasiparticle energy for the highest occupied molecular orbital (HOMO). Higher ionization energies are obtained from deeper molecular orbitals. As reference, we show in Fig. 2 the prediction from LDA (i.e., negative of the Kohn-Sham eigenvalues for occupied orbitals), although such comparison should be made with caution since, from a strict point of view, such eigenvalues enter in DFT as mathematical entities, with no explicit physical meaning. By extending Koopman's theorem to DFT, the HOMO eigenvalue can be shown to be equal to the first ionization potential if the exact functional is used⁴⁹, but such property does not hold for higher ionization potentials^{49,50}. Hybrid functionals⁵¹ and the ones of the exact-exchange type^{52,53} can give very good predictions for the first ionization potential.

In contrast, quasiparticle energies do have physical meaning, and Fig. 2 shows definite consistency between theory and experiment. In particular, the first ionization energy is predicted to be 9.30 eV within GW_f , with remarkable agreement with the experimental value of 9.3 eV^{46,54} and also with the prediction from quantum chemistry calculations: 9.04 eV⁵⁵. A hybrid B3LYP functional predicts 9.74 eV for this ionization energy⁵⁶. The GW_0 approximation predicts the same quantity to be 9.88 eV. The difference is due mostly to the vertex term: the contribution Γ_f for the HOMO alone is found to be almost 0.8 eV, while LDA exchange-correlation corrections in the polarizability give a contribution somewhat smaller but of opposite sign. For other quasiparticle energies, the vertex term is always positive (i.e., it lowers the ionization energy compared to the GW_0 value), and no more than 1 eV.

Ionization energies in the range of 20 to 25 eV are found to be systematically underestimated with respect to experiment, as shown in Fig. 2. For such deep orbitals, we expect to have some loss of numerical accuracy since, although the energy dependence of the polarizability Γ_f is exactly calculated using Eq. (2), the summation over s is always limited to a finite number of poles.

The quasiparticle energy for the lowest unoccupied molecular orbital (LUMO) is the negative of the electron affinity^{3,8}, and its calculated value is shown in Table I. Although the anion $C_6H_6^-$ is unstable, Burrow and collaborators⁵⁸ have been able to perform careful electron transmission experiments and identify resonances in the spectrum, which were associated to the electron affinity. Two resonances were found: at energies 1.12 eV and 4.82 eV. They match theoretical predictions from the GW_f approximation both in energy and spacial distribution: e_{2u} () and b_{2g} () respectively. Again, there is a discrepancy between GW_0 and GW_f quasiparticle energies of about 0.5 eV, mostly due to vertex corrections in

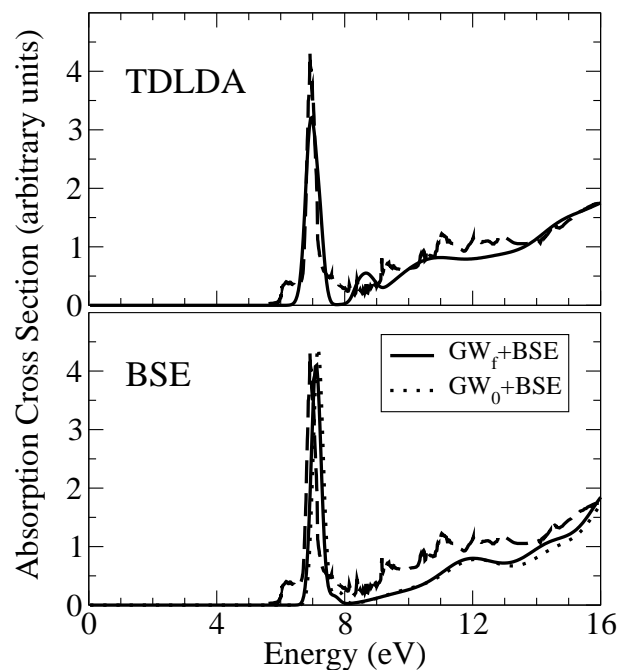


FIG. 3: Absorption spectrum of benzene, calculated within TDLDA (upper panel) and BSE (lower panel). Absorption lines were broadened by Gaussian convolution with dispersion 0.15 eV (below 10 eV) and 0.5 eV (above 10 eV). The measured spectrum⁶¹ is shown in dashed lines. In the lower panel, the BSE was solved using two approximations for the self-energy: GW_0 (dotted line) and GW_f (solid line).

the self-energy.

If measuring electron affinities of benzene is not trivial, a similar statement can also be made regarding first-principles calculations. The anion $C_6H_6^-$ is correctly predicted within DFT to be unstable, and methods such as SCF (energy variations in self-consistent eld) fail to predict its electron affinity²⁶. Indeed, confining the anion inside a spherical boundary of radius R and solving the Kohn-Sham equations results in an excess energy relative to the neutral system that is proportional to R^{-2} . This excess energy vanishes in the limit of very large radius. The physical picture is that, although the anion is unstable, it can be detected as a resonance if electrons do

TABLE I: Electron affinities in benzene, as predicted within GW_0 , Eq. (22) and GW_f , Eq. (29). The outer-valence Green's function (OVGF) method⁵⁵ is based on a Hartree-Fock expansion of the self-energy, combined with self-consistent calculations of self-energy and Green's function. All energies in eV.

	LDA	GW_0	GW_f	DFT (B3LYP) ⁵⁷	OVGF ⁵⁵	Exp. ⁵⁸
e_{2u} ()	1.33	-0.47	-0.99	-0.88	-2.605	-1.12
b_{2g} ()	-2.45	-4.49	-5.05			-4.82

TABLE II: Excitation energies of the lowest-energy neutral excitations in benzene. Energies in eV.

	TDLDA	GW ₀ +BSE	GW _f +BSE	TDDFT (B3LYP) ⁶³	TDDFT (LHFX) ⁵²	CASPT2 ⁶²	Exp. ⁶⁴
Triplet							
B _{1u}	4.53	3.59	3.59	4.45	4.27	3.89	3.9
Singlet							
B _{2u}	5.40	4.74	4.86	5.24	5.40	4.84	5.0
B _{1u}	6.23	6.08	6.14	6.09	6.12	6.30	6.2
E _{1u}	6.9-7.2	7.16	7.23	6.90	6.96	7.03	6.9

not remain in their ground state, and the GW approximation predicts that resonance as a quasiparticle orbital.

As mentioned in the context of Eq. (32), quasiparticle wave-functions are obtained by numerically diagonalizing the quasiparticle Hamiltonian, and therefore they are different from Kohn-Sham eigenfunctions. For the benzene molecule, we observed though that quasiparticle and Kohn-Sham eigenfunctions overlap by more than 95 % for all occupied orbitals. This is due to the high symmetry of the benzene molecule, which makes most off-diagonal matrix elements of the self-energy zero by selection rules. Similarly, the resonant states e_{2u} and b_{2g} in Table I have overlaps of 99 % and 63 % respectively. For them, overlap is still suppressed by selection rules but the existence of many low-energy, unbound orbitals makes overlap somewhat more favorable for orbitals well above the HOMO-LUMO gap.

Optical excitations were obtained in two methods: both within TD L D A and by solving the B S E. Fig. 3 shows the cross section for photoabsorption in benzene. It is dominated by a sharp and well pronounced peak at around 7 eV, as verified by various calculations^{20,47,59,95}. This peak is the visible component of a complex, originated from transitions between the HOMO and the quasiparticle state e_{2u} . The low, at feature in the 6.0-7.0 eV range is due to coupling between π transitions and vibrational modes^{47,60}, and it is absent in the calculated spectra because of the assumed structural rigidity. Beyond 10 eV, a number of sharp features in the measured spectrum results from transitions involving Rydberg states^{60,61}. The limited numerical accuracy in that energy range prevents a detailed identification of such transitions in the calculated spectrum.

Table II shows a comparison between TD L D A and B S E predictions for some excitations in the π complex, together with CASPT2 calculations⁶² and other TDDFT calculations^{52,63}. Although singlet transitions B_{1u}¹ and E_{1u}¹, which are the dominant ones in the low-energy part of the absorption spectrum, are equally well described by both methods, there is a significant blue shift of dark transitions B_{1u}³ and B_{2u}¹ within all TDDFT approaches presented. With the exception of the E_{1u}¹ transition, excitation energies obtained by solving the B S E are typically underestimated with respect to mea-

sured quantities. The overall deviation between measured transition energies and GW predictions is 0.1 to 0.3 eV, comparable to CASPT2 results⁶².

Although excited states can be obtained from either TD L D A or B S E by solving suitable eigenvalue problems, these two theories provide very different descriptions for "electron-hole" correlations. Within TD L D A, such correlations are included in the exchange-correlation kernel, which is static and local in space. Within B S E, they are included both in quasiparticle energies (through the self-energy operator) and in the kernels K^d and K^f . And these differences manifest themselves in a very intriguing way in the π complex: both theories agree within 0.1 eV in the excitation energy of components B_{1u} and E_{1u}, but they differ by more than 0.5 eV in the excitation energy of component B_{2u}.

As observed in Fig. 2 and Table I, the inclusion of vertex corrections together with a TD L D A polarizability is essential for an accurate prediction of the ionization po-

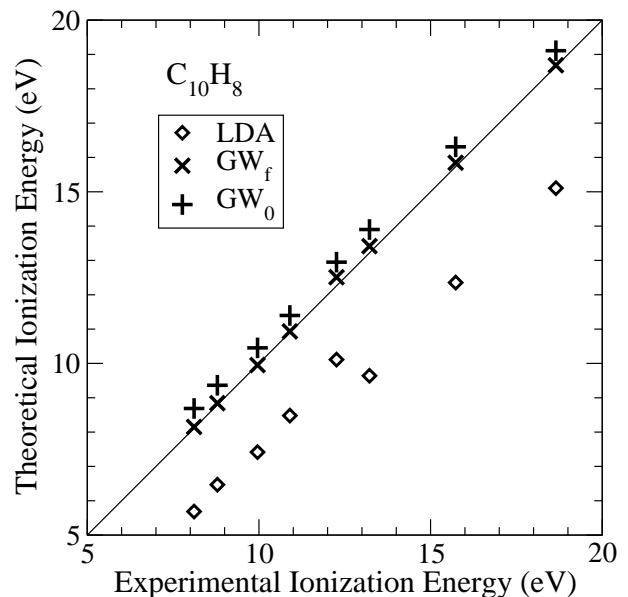


FIG. 4: Ionization energies of naphthalene, associated to all occupied orbitals and the rest orbitals in the molecule. Experimental data from⁶⁷.

TABLE III: Electron affinities in naphthalene, Energies in eV.

	LDA	GW ₀	GW _f	DFT (B3LYP) ⁵⁷	OvGF ⁵⁵	Exp. ⁵⁸
b _{1g}	1.38	-0.09	-0.60			-0.90
b _{2g}	2.19	0.64	0.14	-0.20	-1.30	-0.19
b _{3u}	0.76	-1.07	-1.35			-1.67
a _u	-1.14	-3.03	-3.44			-3.38

tential and electron affinity of benzene. In fact, the GW₀ approximation predicts those quantities to be 9.84 eV and -0.54 eV respectively. Defining a "HOMO-LUMO gap" as the difference between ionization potential and electron affinity, both GW₀ and GW_f approaches agree in the value of the gap: 10.3 eV. This is somewhat consistent with the observation by delSole and collaborators³⁸, who conducted a similar analysis in bulk silicon and found significant shifts in the valence band maximum and conduction band minimum, but only small change in the energy gap itself. Due to the cancellation of vertex contributions, the energy position of the line is not significantly affected by the choice of self-energy approximation in the solution of the BSE, as shown in the lower panel of Fig. 3.

Naphthalene, C₁₀H₈ is the second smallest oligoacene. For this molecule, we used the following parameters in the solution of the Kohn-Sham equation: grid spacing 0.4 a.u., boundary radius 20 a.u., and experimental values of bond length. Ionization potentials associated to all occupied orbitals and some orbitals were reported by Dewar and Worley⁶⁷, with the first one being 8.11 eV. Some of the theoretical calculations of the first ionization potential are: 7.85 eV (OvGF method⁵⁵); and 7.59 eV (hybrid B3LYP/DFT⁶⁸). Predictions from the GW_f and GW₀ approximations are 8.15 eV and 8.69 eV respectively. Fig. 4 presents a comparison between predictions from the GW_f and GW₀ approximations for all other potentials. Although both are acceptable, the GW_f approximation is clearly superior to GW₀, giving a maximum deviation from experiment of no more than 0.3 eV. Vertex corrections are of the order of 0.6 eV. We should point out that the magnitude of self-energy corrections for orbitals (experimental ionization energy ranging from 8 to 13 eV⁶⁷) is around 2.4 eV, whereas the self-energy corrections for orbitals (experimental ionization energy ranging from 13 to 19 eV⁶⁷) is bigger: around 3.6 eV. Since orbitals are typically deeper in energy than , they are expected to have self-energy corrections larger in magnitude.

There has been some debate in the literature concerning the stability of the anion C₁₀H₈⁶⁹. Early electron capture experiments have observed a stable anion with electron affinity in the range of 0.15 eV⁷⁰. In contrast, electron transmission spectroscopy measurements have indicated the ion to be unstable, with negative electron affinity of -0.2 eV⁵⁸. The anion is predicted by GW_f

to be stable, with electron affinity of 0.14 eV. Table III presents a comparison between the calculated electron affinities and the experimental data⁵⁸. The fact that the anion has such small binding energy makes any stability analysis, either from theory or experiment, very difficult. As observed in benzene, there is a number of low-energy orbitals around the LUMO, most of them highly delocalized. But some of those orbitals are localized around the molecule, and they are responsible for the resonant states detected in electron transmission spectroscopy measurements⁵⁸. For the resonant states, we find fair agreement in terms of orbital character and corresponding electron affinity, although there is a discrepancy of typically 0.2 to 0.3 eV in the last quantity.

The absorption spectrum of naphthalene is found to have a sharp and well-pronounced line at 6.0 eV. This line is originated from a B_{1u} transition which is optically active for light polarization along the line that joins the centers of the two aromatic rings in the molecule, called "long molecular axis". A second, lower absorption line is located at 4.3 eV and it has B_{2u} character, being highly active for polarization on the plane of the molecule but perpendicular to the long molecular axis. TD-LDA and BSE give very similar values for the energy position of both lines, although they differ by 0.5 eV in the predicted value of the first excited state, a dark B_{1u} singlet excitation. A comparison between the theoretical calculations and experimental data is shown in Table IV.

In summary, the absorption spectra of benzene and naphthalene are dominated by a sharp transition, found in both TD-LDA and GW+BSE methodologies. Considering that this transition is composed of hybridized carbon-p orbitals, it is expected to be very localized in space. We do not discard the possibility of strong spacial localization being a major reason for such good agreement between TD-LDA and GW+BSE, despite the conceptual simplicity of the former. The good agreement between predicted and measured ionization potentials of benzene and naphthalene is equally remarkable. There has been a very limited number of cases where such quantities were calculated within the framework of the GW approximation^{4,8,9,17,18,19}, and the present results provide the first benchmarks for ionization potentials in oligoacenes.

TABLE IV : Excitation energies of the lowest-energy neutral excitations in naphthalene. Spin-singlet states only. Energies in eV.

	TD LDA	GW ₀ +BSE	GW _∞ +BSE	TDDFT (B3LYP) ⁶³	CA SPT 2 ⁶⁵	Exp. ⁶⁶
B _{1u}	4.40	3.93	4.02	4.21	4.03	3.97
B _{2u}	4.32	4.28	4.34	4.12	4.56	4.45
B _{1u}	5.84	6.04	6.12	5.69	5.54	5.89
B _{2u}	6.13	6.08	6.16	5.90	5.93	6.14

B. Silicon clusters

Small semiconductor clusters containing a few tens of atoms and with various chemical compositions have been mass produced and characterized in terms of their optical properties and structural conformation, although the synthesis of small silicon clusters remains a challenging task^{14,71,72}. From a theoretical point of view, optical properties of small silicon clusters are interesting for one aspect: the linear optical spectrum of bulk silicon is known to be extremely well predicted by a first-principles approach based on the BSE^{7,8}, whereas TD LDA fails to predict both the optical gap and excitonic effects^{21,73,96}. On the other hand, optical excitations of SiH₄ and Si₂H₆, the two smallest "clusters", are correctly described within TD LDA²⁰. Based on these two facts, it is natural to investigate what limits the validity of each theory and where the crossover size is, beyond which one theory becomes superior to the other. Such an analysis is challenging because of two major factors: the limited number of useful experiments, and the complexity of some numerical implementations of the BSE method. Recently, a study based on model dielectric screening in silicon clusters have addressed the issue, with inconclusive results¹⁸. Since the present implementation of the BSE method is particularly efficient for finite systems, we are able to compare both TD LDA and BSE methods in a wide range of cluster sizes and with a minimum of ad hoc assumptions. As we discuss below, there is unfortunately one additional difficulty in such comparisons: there is no direct relationship between the optical spectrum of a nanostructure (quantified by the absorption cross section, for instance) and the optical spectrum of a macroscopic solid (quantified by the macroscopic dielectric function).

In general, the surface of synthesized silicon clusters is covered by passivating particles and, for the smallest ones, they may undergo significant reconstruction⁷². Our approach is to construct clusters from fragments of crystalline silicon and adjust the number of atoms so that the fragment has surface as spherical as possible. Dangling bonds on the surface are passivated by attaching hydrogen atoms. We do not consider surface reconstruction. Although the class of tetrahedral clusters we discuss here may not be the most stable ones in the size range of 0 to 2 nm, they are expected to be the most stable ones when the cluster size is very large. Here, we ana-

lyze the clusters SiH₄, Si₅H₁₂, Si₁₀H₁₆, Si₁₄H₂₀, Si₂₉H₃₆, Si₃₅H₃₆, Si₄₇H₆₀, Si₇₁H₈₄, Si₉₉H₁₀₀, and Si₁₄₇H₁₀₀. Since the presence of hydrogen atoms typically requires dense grids, we use grid spacings ranging from 0.5 a.u. (SiH₄) to 0.7 a.u. (Si₁₄₇H₁₀₀) in the solution of the Kohn-Sham equations.

For each cluster, the quasiparticle Hamiltonian is re-orthogonalized in the Kohn-Sham basis. As emphasized in the literature^{8,17}, the self-energy operator is not diagonal, and Kohn-Sham eigenfunctions are not good approximations for quasiparticle wave-functions, particularly for the low-energy unoccupied orbitals in the smallest clusters. There are two main reasons for this phenomenon: LDA wrongly predicts some of these unoccupied states to be bound, whereas quasiparticle orbitals are often unbound and more extended; and the large density of orbitals within a few eV from the LUMO makes the occurrence of non-negligible off-diagonal matrix elements of the operator in Eq. (32) very frequent. The Si₃₅H₃₆ cluster is a typical example. There, overlap between Kohn-Sham and quasiparticle wave-functions is observed to be greater than 95% for most occupied states and for the first few unoccupied ones, but it reduces to values ranging from 30% to 90% for the higher-energy unoccupied states.

One important aspect involving self-energy corrections is whether they can be modeled by a "scissors" operator or not. Frequently, the quasiparticle band structure of solids differs from the one predicted within LDA by a rigid upward shift of conduction bands with respect to valence bands^{2,4}, which justifies the scissors approximation. Scissors operators with energy dependence can also improve band widths⁴. But we find this procedure to be inaccurate even for moderately large clusters. Fig. 6 shows diagonal matrix elements of the self-energy operator as function of the LDA energy eigenvalue for all occupied orbitals and some unoccupied orbitals of Si₃₅H₃₆. For deep occupied orbitals, these matrix elements follow a quasi-continuous distribution, with smooth curvature, so a scissors operator could be defined. But the matrix elements for orbitals in the vicinity of the energy gap do not have a well-defined dependence with respect to LDA eigenvalues. On the contrary, they have strong orbital dependence. This fact, together with the existence of large off-diagonal matrix elements, makes any attempt at constructing a scissors operator very difficult for these clusters.

Fig. 5 shows the dependence of electron affinity and first ionization potential with respect to the cluster diameter. To our knowledge, the ionization potential has not been measured for any of the studied clusters except for SiH_4 , for which the experimental value is 12.6 eV⁷¹. For this system, the prediction from GW_ϵ is 12.5 eV. Starting from SiH_4 , the first ionization potential decreases monotonically as the cluster size increases. On the other hand, the electron affinity remains very small, with little dependence with respect to cluster size. As a result, the electronic gap (defined as the difference between ionization potential and electron affinity) decreases continuously for larger and larger clusters. This is a size effect which has been observed before for small clusters⁸. In order to understand the physics behind it, we model the cluster as an electron sphere with homogeneous density and radius R , keeping the density constant and proportional to $N=R^3$. The energy of the HOMO is found by integrating the density of states up to the number of electrons N , resulting in $E_F = \text{const} \cdot N^{2/3} R^{-2}$. The energy difference between this orbital and the next one is approximately $E = \text{const} \cdot N^{-1/3} R^{-2} = \text{const} \cdot R^{-3}$, which is inversely proportional to the volume of the cluster. A more elaborate analysis predicts a power law R^{-2} instead of R^{-3} ⁷⁴.

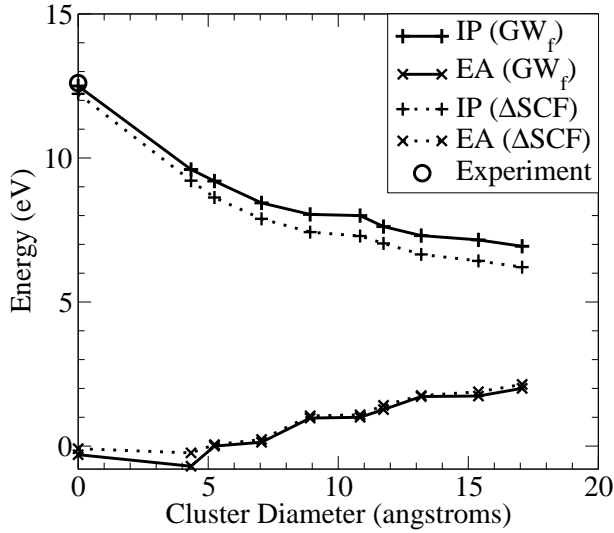


FIG. 5: First ionization potential and electron affinity of passivated silicon clusters, calculated within the GW_ϵ approximation (solid lines) and SCF (dotted lines). Experimental data from Ref.⁷¹. SCF results include spin-polarization effects.

We observe a systematic discrepancy in the first ionization potential as predicted within GW_ϵ and SCF, the difference being 0.6 to 0.9 eV throughout the range of studied cluster sizes. In contrast, the electron affinity shows better agreement between these two theories. Possible explanations for this behavior are the spurious self-interaction effect, present in SCF calculations, and the incorrect asymptotic behavior of the LDA functional^{1,75}.

Fig. 7 shows the absorption cross section for clusters SiH_4 to $\text{Si}_{47}\text{H}_{60}$. The cross section also has a characteristic behavior as function of cluster size: for small clusters, it has a small number of well-defined peaks but, as size increases, their intensity decreases in the low end of the energy axis. For large clusters, the absorption cross section shows a smooth and featureless profile, with onset at a low energy value and continuous increase towards higher values of energy. Also, TD-LDA and BSE spectra are significantly different for small clusters. In particular, TD-LDA predicts a sharp line at around 8.2 eV, whereas the sharp line in BSE is positioned at 9.4 eV. Previous BSE calculations have predicted 9.0 eV⁷⁶ and 9.16 eV⁸ for the same quantity. The experimental value has been reported to be around 8.8 eV⁷¹. For bigger clusters, the differences between TD-LDA and BSE tend to disappear.

As pointed out recently¹⁸, the behavior of the absorption cross section for large clusters is dictated by the exchange kernel $K_{vcv'c'0}^x$, which is present in both TD-LDA and BSE formalisms. This term introduces a long-range interaction that increases in strength as function of cluster size and ultimately dominates both the exchange-correlation kernel in the TD-LDA eigenvalue equation and the direct+vertex kernel in the BSE. As a result, oscillator strength is redistributed among the excited states of the system and the absorption spectrum peaks at frequencies well above the optical range. Differences in the detailed treatment of electron-hole correlations, intrinsic to both TD-LDA and BSE, are expected to be less and less important for increasingly large clusters.

As the cluster size increases, more transitions become allowed and the absorption cross section is expected to evolve into a well-pronounced and broad peak at the plasmon-pole frequency. Indeed, the formalism in Sections IIIA and IIC can be applied directly to solids. In

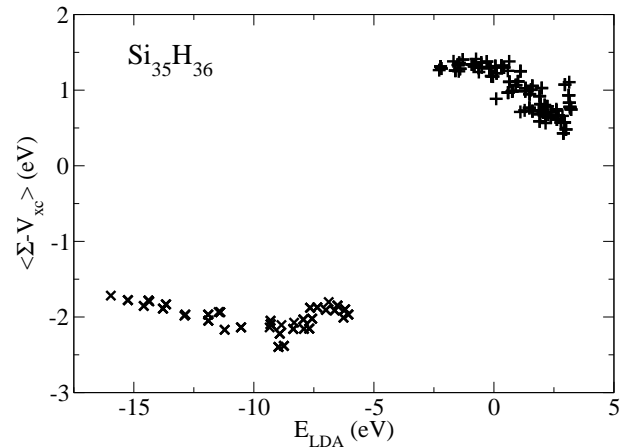


FIG. 6: Diagonal matrix elements of the operator ΣV_{xc} , c.f. Eq. (32), evaluated in the basis of Kohn-Sham eigenfunctions. Matrix elements for occupied (unoccupied) orbitals are represented by crosses ("plus" signs). Self-energy is evaluated within the GW_ϵ approximation and at the extrapolated quasiparticle energy (see text).

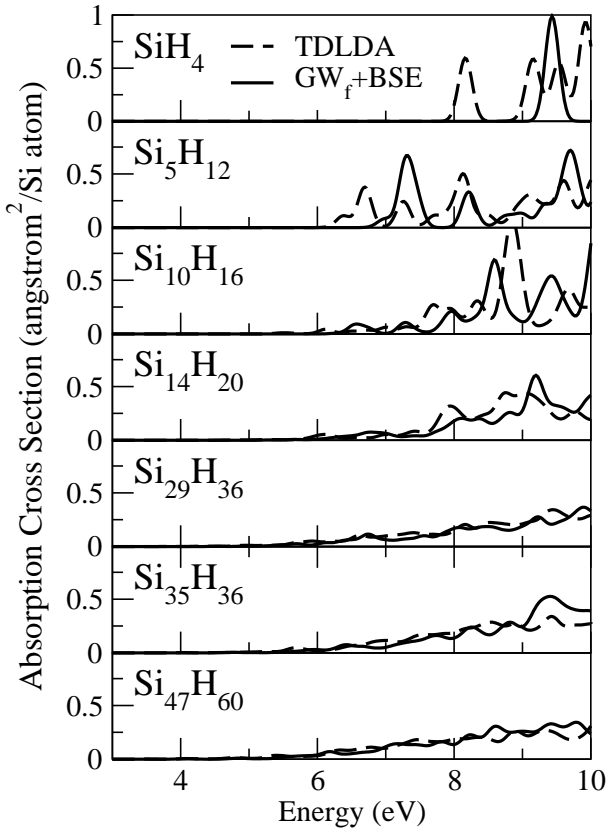


FIG. 7: Cross section for photoabsorption in passivated silicon clusters, calculated within TDLDA (dashed lines) and BSE (solid lines). The self-energy operator used in BSE is calculated within the GW_f approximation. The cross section is normalized by the number of silicon atoms in each cluster. Absorption lines were broadened by a Gaussian convolution with dispersion 0.1 eV.

solids, Eq. (11) reduces to a function proportional to the imaginary part of the inverse dielectric function, measurable by electron energy loss spectroscopy, EELS. Olivano and Reinig⁷⁷ have shown that the random-phase approximation correctly predicts the essential features of the EELS of bulk silicon, and including corrections at BSE level does not lead to substantial improvements. As expected, the spectra of the largest clusters studied, depicted in the lower panels of Fig. 7, show a smooth profile typical of the low-energy end of the plasmon peak.

The blue shift can be discussed in terms of classical electrodynamics. We consider a material composed of several identical, spherical particles in suspension inside an optically inert background. According to the Mie theory (or effective medium theory)^{25,78}, the (macroscopic) dielectric function of the medium is size-dependent, and there are three important regimes: particles much smaller than the wavelength of light; particles of size comparable to the wavelength of light; and particles much bigger than the wavelength of light. In the regime of small particles in very low concentration, the imaginary part of the dielectric function is proportional to the absorption

cross section of each particle according to the expression

$$\epsilon_2 = n^2 \epsilon_1 \quad ; \quad (41)$$

where λ is the wavelength of light and n is the concentration. The two functions then share the same energy dependence. This is a special case of the Clausius-Mossotti relation when $n \neq 0$. In denser medium, the proportionality above no longer holds and the energy dependence of ϵ_2 is now given by a non-linear Clausius-Mossotti relation. In the extreme situation of highly packed particles, with no interstices, the function ϵ_2 should resemble the bulk dielectric function. As the particles condense, any similarity between the energy dependencies of ϵ_2 and ϵ_1 is lost. The qualitative aspects of this analysis still hold for more complicated cases, such as non-spherical and/or inhomogeneous particles. Some predictions of the Mie theory for the optical properties of nanostructures have been discussed in recent first-principles calculations: the emergence of a Mie plasmon in nanoclusters⁷⁹; and the dependence of dielectric function with respect to concentration in periodic arrangements of nanowires⁸⁰.

In Fig. 7, the parameter is particle size rather than concentration. From the calculated spectra, one can recover the bulk limit by increasing the concentration or the size of particles. In the first case, the Mie theory predicts a red shift of ϵ_2 with respect to ϵ_1 . The second case should certainly involve a similar phenomenon but it requires a more elaborate analysis, because of the crossover between particle size and wavelength. The crossover does not necessarily affect the absorption cross section because light is not an essential element in absorption measurements (for instance, one can use electron beams instead of photons as probe). But it should affect the dielectric function because measurements of dielectric function necessarily involve interaction with photons.

Although the behavior of the absorption cross section is well understood, we conclude that spectra of large clusters are not directly related to the macroscopic dielectric function. Whereas excitonic effects and optical band gaps are easily recognized in the macroscopic dielectric function, the same does not hold for the inverse dielectric function. In principle, these two functions are linked by simple inversion^{3,7,31}, but the delicate features of both functions can be lost if numerical inversion is attempted without careful control of numerical accuracy. For solids, numerical inversion is avoided by replacing the BSE for the polarizability operator with a similar equation that, when solved, provides the macroscopic dielectric function directly^{7,81}. For confined systems, no such prescription is known, and therefore the question of how to compute an absorption spectrum that, in the bulk limit, reduces unambiguously to the macroscopic dielectric function remains unanswered.

The problem of an indeterminate crossover and ill-defined bulk limit in the absorption spectrum has two important consequences. The first one is that the identification of excitonic effects in large silicon clusters becomes a non-trivial task, even if the cluster is sufficiently

large so that the very concept of "exciton" applies. The second is that an optical gap cannot be easily extracted from the absorption cross section of large clusters. As seen in Fig. 7, the onset of absorption for the large clusters is not well defined. Often, low-energy excitations in the cluster have extremely small oscillator strength and they should not be used to define a gap. Presently, one tentative definition of the optical gap is via a threshold approach: the optical gap E_G is such that the integrated cross section up to E_G is a fixed fraction of the total integrated cross section²⁰:

$$\int_0^{E_G} \sigma(E) dE = p \int_0^{E_1} \sigma(E) dE; \quad (42)$$

where p is a small fraction. This prescription is motivated by experiment: often, the onset of absorption cross section cannot be distinguished due to limitations in experimental resolution, and a practical definition of optical gap becomes important. An obvious drawback of Eq. (42) is that the gap may be sensitive to the choice of p . In practice, this prescription has been observed to be robust²⁰.

In Fig. 8, we show the minimum gap and optical gap as predicted within TD-LDA and BSE. The minimum gap is defined as the energy of the lowest excited state, irrespective of oscillator strength, whereas the optical gap is defined from Eq. (42) with $p = 2 \times 10^{-4}$. As expected, both gaps have strong dependence with respect to cluster size. In addition, the BSE gaps are typically larger than the corresponding TD-LDA ones, the difference slowly decreasing for larger clusters and almost vanishing for $\text{Si}_{147}\text{H}_{100}$. Fig. 8 also shows that the difference between TD-LDA minimum and optical gaps has a slow tendency towards increasing with cluster size, but the same is not observed in the BSE gaps. The reason for this behavior is that low-energy excitations obtained within BSE have larger oscillator strengths than the corresponding ones in TD-LDA. Discrepancies between the TD-LDA optical gap in Fig. 8 and previous work²⁰ is due to different choices for the value of p .

The dependence of the minimum gap with respect to cluster size has also been discussed in the context of quantum Monte-Carlo (QMC) calculations⁸³. QMC and GW + BSE share a common link: both of them are many-body theories, and therefore they both include correlation effects not present in TD-LDA. A signature of these effects can be recognized in the calculated minimum gap: QMC and GW + BSE give similar values for that quantity, both of them overestimated with respect to TD-LDA (c.f. Fig. 8 and Ref.⁸³). For large clusters, there is a tendency for the QMC gap to fall above the GW + BSE gap. For instance, the GW + BSE minimum gap for $\text{Si}_{147}\text{H}_{100}$ is found to be 3.3 eV, whereas QMC predicts a gap of around 4 eV⁸³. The corresponding gap within TD-LDA is found to be 2.5 eV.

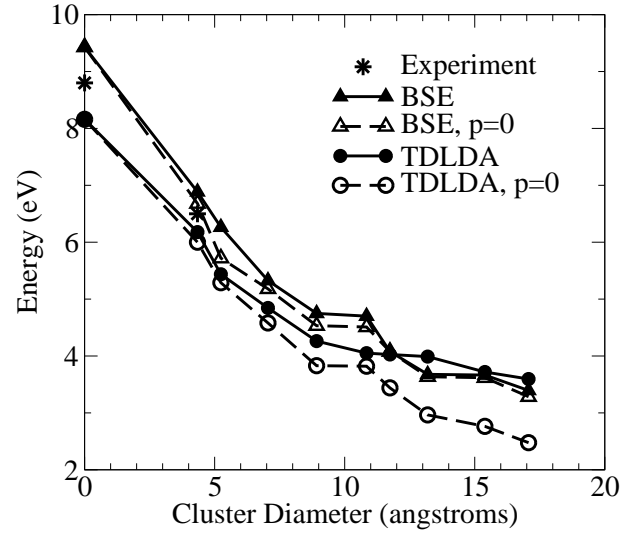


FIG. 8: Minimum gap (dashed lines and open symbols) and optical gap (solid lines and filled symbols) for passivated silicon clusters. Circles denote TD-LDA gaps. Triangles denote GW + BSE gaps. The optical gap is obtained by integrating the oscillator strength up to $p = 2 \times 10^{-4}$. The minimum gap is defined as the lowest spin-singlet excitation energy ($p = 0$) in the system. Experimental data from Refs.^{71,82}.

C. F-center defects in LiCl

The formalism presented in Section IIB can also be applied to extended systems, once the appropriate boundary conditions are used in the solution of the Kohn-Sham equations⁸⁴. In fact, the boundary conditions imposed on electron wave-functions determine the ones for the polarizability operator, through Eqs. (2), (3), (39), and (40). In periodic systems, optical absorption is quantified by the absorption coefficient, or by the imaginary part of the macroscopic dielectric function. Here, we calculate this dielectric function following an approach due to Hanke^{7,81}. The basis of this approach is in defining a truncated Coulomb potential \hat{V} in the construction of the exchange kernel K^x :

$$K_{\nu c \nu' c'}^x \neq K_{\nu c \nu' c'}^x = K_{\nu c \nu' c'}^x \frac{4 e^2 \hbar v_j}{N_k V_{\text{cell}}} \frac{v_j \cdot \mathbf{c}^0}{v_j \cdot \mathbf{c}^0} \frac{v_j \cdot \mathbf{c}^0}{v_j \cdot \mathbf{c}^0};$$

where v is the velocity operator projected along some direction \mathbf{c} . The volume of the periodic cell, V_{cell} and number of k -points, N_k , are included as normalization factors. The kernel \hat{K}^x in the above equation does not have direct physical meaning, being rather an auxiliary quantity, which differs from the original K^x by the absence of a long-range Coulomb interaction. By using this truncated kernel, Hanke has shown⁸¹ that a polarizability operator can be obtained and, from that, the macroscopic dielectric function according to

$$\text{Im } f_{\mathbf{q}} = \frac{4}{N_k V_{\text{cell}}} \sum_{\mathbf{s}} \frac{e^2}{\epsilon_{\mathbf{s}}} \sum_{\mathbf{j}} \int d\mathbf{r}_s(\mathbf{r}) \mathbf{v}_{\mathbf{j}}^2(\mathbf{E}_{\mathbf{s}}) ; \quad (43)$$

where $\epsilon_{\mathbf{s}}$ and $\mathbf{v}_{\mathbf{j}}$ can be found by diagonalizing either TD-LDA-like or BSE-like eigenvalue equations^{7,73,81}. In addition, lattice periodicity allows us to use a wave-vector \mathbf{q} as additional quantum number in the polarizability. Each choice of \mathbf{q} leads to a different eigenvalue equation and the resulting partial polarizabilities are summed up.

Here, we are interested in analyzing the optical spectrum of a F center embedded in an otherwise ordered LiCl crystal. F centers are halogen vacancies found in alkali-halide crystals, and they are named after the bright, visible coloration they induce. Alkali-halide crystals are well-known for their strong ionicity and wide energy gap, which makes them transparent to visible light. Halogen vacancies induce localized electronic states inside the gap, and electronic transitions involving such localized states are the source of the bright color in F-center-rich crystals. The nature of F centers has been studied experimentally using various techniques⁸⁵.

From a theoretical point of view, F centers are challenging because the exact location of defect states inside the gap is not easily obtained without experimental input. Effective-mass models are not suitable due to the extremely large band gap, high effective masses, and small dielectric constant. Also, DFT suffers drawbacks due to the intrinsically underestimated band gap. Within the GW approximation, not only the band gap is correctly predicted, but defect states around the F center in LiCl can also be located⁸⁶. Here, we go beyond and determine optical excitations and the dielectric function within BSE, and compare the results with the TD-LDA prediction and with experiments.

Defect levels in LiCl are extremely localized, which simplifies considerably the numerical work. We simulate the defect by using a cubic supercell with 32 lithium and 32 chlorine atoms. The lattice parameter is taken from experiment. Starting from the ordered structure, one chlorine atom is removed and the Kohn-Sham equations are solved in real space with grid spacing 0.3 a.u. All atoms inside the periodic cell are allowed to move so as to minimize the total energy. Only atoms in the first lithium shell showed significant relaxation, with displacement of 0.05 a.u. and relaxation energy 30 meV. As a convergence test, the procedure was repeated in a much bigger cell, containing 216 atoms of each type (excluding the vacancy). Movement of atoms in the first shell was around 0.02 a.u. and relaxation energy less than 10 meV, thus showing the degree of localization of the defect. In the subsequent work, we used the 32Li+32Cl vacancy cell. Since the presence of a vacancy breaks translational invariance, we reduced the Brillouin zone to the Γ point only, thus removing complications with Bloch functions and integrations over the Brillouin zone⁸⁴.

Quasiparticle energies for the band edges and two de-

TABLE V: Electron band structure of the F center in LiCl, with defect levels. All calculated energies are given with respect to the valence band maximum as predicted by GW_F, in eV. Results obtained from a 2x2x2 cubic supercell, containing 63 atoms. Defect level 2p has a spin splitting of 0.4 eV. Results in column "GW bulk" were obtained by Hybertsen and Louie² for bulk LiCl.

	LDA	GW _F +BSE	GW bulk ²	Exp. ^{85,90}
L _v	0.43	-0.21	0.3	
v	0.64	0	0	0
1s	5.19	6.37		
2p	8.11	10.4-10.8		
c	6.96	9.35	9.1	9.4
L _c	7.06	9.63	9.7	
X _c	8.29	10.90-10.7		

fect levels are shown in Table V. The choice of supercell allows us to recognize easily the band edges at points Γ , L, and X by observing the symmetry properties of the calculated single-particle orbitals. Self-energy corrections in the neutral F center require the explicit inclusion of spin degrees of freedom: the 1s state is partially occupied with only one electron. Therefore, the self-energy operator was evaluated separately for the two possible spin configurations and the summation over occupied states in Eq. (23) performed over all occupied states for each spin configuration. A similar procedure was used for the evaluation of the correlation and vertex parts of the self-energy. Although the self-energy operator is spin-dependent, most quasiparticle levels remain spin-degenerate, which is expected since there is no intrinsic source of spin polarization in the system. Table V shows that, within DFT-LDA, the 1s state is positioned inside the gap, but the 2p triplet state is located within the conduction band. Inclusion of self-energy corrections keeps the 2p triplet above the conduction band maximum (CBM). This phenomenon has been observed before⁸⁶. Although mixed with extended states, the 2p triplet remains fairly localized within the vacancy. Indeed, 45% of its probability distribution is located within a distance of L_0 or less from the vacancy, where L_0 is the Li-Cl interatomic distance. For comparison, 74% of the 1s probability distribution is located within the same region.

Optical excitations in the system are calculated in both TD-LDA and BSE frameworks. In both cases, spin polarization is included explicitly in the construction of the electron-hole kernel. Although not essential at TD-LDA level, the inclusion of spin polarization is important in the BSE because of the existence of the 1s partially occupied orbital. Fig. 9 shows the imaginary part of the dielectric function for the cubic supercell containing 63 atoms. Although this crystal has an electronic band gap of 9.4 eV, the BSE spectrum is dominated by a wide double peak just below 9 eV. Being located below the band

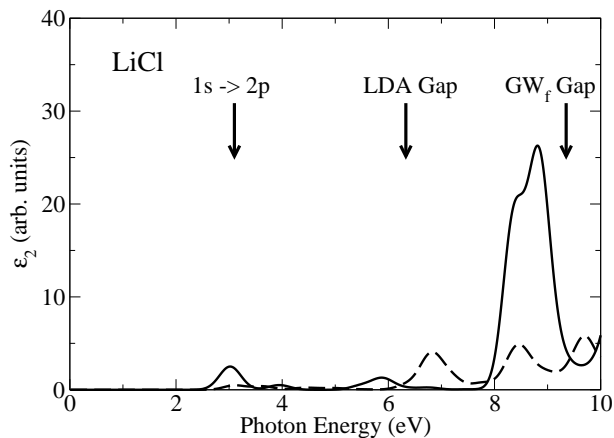


FIG. 9: Imaginary part of the macroscopic dielectric function, ϵ_2 for a F center embedded in LiCl. Solid and dashed lines correspond to $\text{GW}_f + \text{BSE}$ and TD-LDA calculations respectively. The self-energy operator used in BSE is calculated within the GW_f approximation. The position of the $1s \rightarrow 2p$ transition line and electronic bands gaps within LDA and GW_f are shown with arrows. A Gaussian convolution with dispersion 0.2 eV was used to smear out the absorption lines.

gap, this peak has the signature of excitonic effects⁸. The limited supercell size compromises resolution of the excitonic double peak and causes a redshift of 0.2 to 0.4 eV, although the overall features are consistent with calculations for a clean LiCl crystal. Below the excitonic peak, we can see one absorption line corresponding to the $1s \rightarrow 2p$ transition. In the real material, the strength of this line depends on temperature and density of defects, and so the calculated strength is somewhat arbitrary.

The absorption spectrum obtained within TD-LDA is characteristic for the absence of the exciton peak. In fact, it has an onset at the DFT-LDA band gap, around 6.3 eV, followed by a featureless rise towards higher energies. The three wide peaks in Fig. 9, located at 6.4, 8.3 and 9.7 eV are due to extremely limited resolution in the supercell. By including more atoms in the supercell, these peaks are expected to merge into a smooth function. The lack of excitonic effects in TD-LDA has been reported in the literature^{7,18,21}.

Surprisingly, TD-LDA does predict a very accurate value for the $1s \rightarrow 2p$ transition energy: 3.10 eV, compared to 3.04 eV (BSE) and the measured value of 3.25 eV to 3.3 eV^{85,87,88,89}. We believe this is related to the strong localization of both $1s$ and $2p$ orbitals. As discussed before, these orbitals are confined within 1 or 2 atom sites from the vacancy. To some extent, the defect behaves as a confined electronic system, separated from the crystalline background. For transitions internal to this defect, such as the $1s \rightarrow 2p$, the LDA exchange-correlation kernel correctly describes electron-hole interactions. But transitions involving the conduction and/or valence bands are not so well described because the LDA kernel lacks the non-locality present in electron-hole interactions involving extended orbitals. The BSE spec-

trum also shows a low feature at around 5.8 eV, which can be assigned to the $1s \rightarrow L$ line⁸⁹.

IV. CONCLUSION

We discussed an implementation of Green's functions methods developed in the space of single-particle transitions. Contrary to alternative approaches, this procedure does not make use of Fourier analysis, and thus can be applied directly to confined systems, where it is particularly efficient. As an example, we are able to do a full $\text{GW} + \text{BSE}$ calculation of the benzene molecule using a 1.7 GHz IBM Power4 machine in single-process mode in 280 minutes. This task requires no more than 600 MB of CPU memory and the only input required is the geometry of the molecule. Taking advantage of the extreme numerical efficiency of the current implementation, we are able to perform *ab initio* $\text{GW} + \text{BSE}$ calculations of silicon clusters containing more than one hundred atoms.

Electronic screening is included within the TD-LDA, and a corresponding vertex is included for consistency in the diagrammatic expansion. The added terms (TD-LDA vertex + TD-LDA screening) are found to be essential for accurate predictions of electron affinity and ionization potentials of benzene and naphthalene. This is in contrast with previous GW calculations which assume screening at RPA level only but nevertheless provide accurate ionization potentials for small molecules^{8,9,17,19}. The explanation for this apparent contradiction may be that the popularly used plasmon pole models carry information about the exact many-body screening and therefore corrects deficiencies of the RPA.

Besides oligoacenes, the current implementation is used to investigate the absorption cross section of silicon clusters by solving the BSE. We conclude that, while the TD-LDA and BSE differ markedly for small clusters, they agree in the broad features of the spectrum for large clusters. In particular, the dependence of excitation energy as function of cluster size is similar for both theories. The present results are consistent with QMC calculations for the minimum gap of silicon clusters. Excitation energies, ionization potentials and electron affinities calculated within the present method are consistent with experimental data to within a fraction of eV, comparable to chemical accuracy⁹¹. In LiCl, we show how the existence of a F center affects the energy-resolved dielectric function. We also show that TD-LDA predicts correctly the position of the $1s \rightarrow 2p$, despite producing a poor description of excitonic effects.

Acknowledgments

This work was supported by the National Science Foundation under DMR-0130395 and DMR-0551195 and by the U.S. Department of Energy under DE-FG02-89ER45391 and DE-FG02-03ER15491. Calculations

were performed at the Minnesota Supercomputing Institute (MSI), at the National Energy Research Scientific Computing Center (NERSC), and at the Texas Advanced Computing Center (TACC).

APPENDIX A: EVALUATION OF ENERGY INTEGRAL IN EQ. (22)

The derivation of Eqs. (23), (24) and (25) from Eq. (22) follows from standard integration over poles^{3,37}. For completeness, we present here the major steps. We start by defining separate exchange and correlation contributions in Eq. (22):

$$h_{jj}(\mathbb{E}^0)_{jj}^0 = h_{jj}^x_{jj}^0 + h_{jj}^c(\mathbb{E}^0)_{jj}^0 \quad (\text{A1})$$

with

$$h_{jj}^x_{jj}^0 = \int^R dr_1 dr_2' \int_j(r_1) i \frac{d\mathbb{E}}{2} e^{i\mathbb{E}^0} G(r_1; r_2; \mathbb{E}^0 - \mathbb{E})'_{j^0}(r_2) V(r_1; r_2); \quad (\text{A2})$$

and

$$h_{jj}^c(\mathbb{E}^0)_{jj}^0 = \int^R dr_1 dr_2' \int_j(r_1) i \frac{d\mathbb{E}}{2} e^{i\mathbb{E}^0} \int^R dr_3 dr_4 V(r_1; r_3) \epsilon_0(r_3; r_4; \mathbb{E}) V(r_4; r_2); \quad (\text{A3})$$

We assume a quasiparticle approximation for the one-electron Green's function,

$$G(r_1; r_2; \mathbb{E}) = \sum_n \frac{u_n(r_1) u_n(r_2)}{E - \epsilon_n + i\eta^0}; \quad (\text{A4})$$

In the exchange term, Eq. (A2), the only poles present are the ones originated from the Green's function. Therefore, the energy integration is easily replaced with a summation over occupied states only, resulting in Eq. (23). For the correlation term, Eq. (A3), we assume a polarizability operator given by Eq. (2). Now, both G and ϵ_0 contribute with poles below the real energy axis. Collecting them, one arrives at Eq. (24).

APPENDIX B: STATIC REMAINDER IN SELF-ENERGY

In most cases, the summation over n in Eqs. (24) and (30) has slow convergence. This behavior is not unique

to the present implementation and it has also been observed in self-energy calculations when the dielectric matrix is explicitly computed in reciprocal space^{2,4,92}. In that case, converged self-energies were found to require in excess of 100 unoccupied bands in the single-particle Green's function. The convergence rate can be accelerated by truncating this summation at some point and evaluating the remainder within the COHSEX (Coulomb hole + screened exchange) approximation⁴. The COHSEX approximation is essentially a static limit of Eq. (22). Assuming that screening is instantaneous, the polarizability ϵ_0 and the potential W_0 become proportional to a δ -function in time and constant in energy. The integral over energy in Eq. (22) can then be replaced by a sum over poles of the single-particle Green's function. In our implementation, one can recover the COHSEX approximation by imposing $!_s \gg \mathbb{E} - \epsilon_n$ in Eq. (24):

$$h_{jj}^c(\mathbb{E})_{jj}^0 \Big|_{\text{COHSEX}} = 4 \sum_n^{\text{occ}} \sum_s^{\text{P}} \frac{v_{nj}^s v_{nj^0}^s}{!_s} \sum_n^{\text{P}} \sum_s^{\text{P}} \frac{v_{nj}^s v_{nj^0}^s}{!_s}; \quad (\text{B1})$$

The last summation on n is done over all Kohn-Sham eigenstates. We evaluate it exactly by using a completeness relation. Using Eqs. (2), (3), (6) and (25), we obtain:

$$h_{jj}^c(\mathbb{E})_{jj}^0 \Big|_{\text{COHSEX}} = 4 \sum_n^{\text{occ}} \sum_s^{\text{P}} \frac{v_{nj}^s v_{nj^0}^s}{!_s} + \frac{1}{2} \int^R dr' \int_j(r) W(r)'_{j^0}(r); \quad (\text{B2})$$

where

$$W(r) = \frac{1}{2} \int^Z dr^0 \int^Z dr^{\text{occ}} V(r; r^0) \epsilon_0(r^0; r^{\text{occ}}; \mathbb{E} = 0) V(r^{\text{occ}}; r);$$

Eqs. (B1) and (B2) can be used to determine the effect of truncating the sum over n at a value $N \gg n_{\text{occ}}$. The remainder then is

$$R_{jj^0}^c(N) = \frac{1}{2} \int^Z dr' \int_j(r) W(r)'_{j^0}(r) \int^Z dr^0 \int^Z dr^{\text{occ}} V(r; r^0) \epsilon_0(r^0; r^{\text{occ}}; 0) V(r^{\text{occ}}; r) + 2 \sum_{n=1}^N \sum_s^{\text{P}} \frac{v_{nj}^s v_{nj^0}^s}{!_s}; \quad (\text{B3})$$

Although the COHSEX approximation has a level of accuracy lower than the full GW method, the convergence behavior is similar in both approximations if N is chosen sufficiently high. Eq. (24) can then be replaced with

$$h_{jj}^c(\mathbf{E}) \delta_{ij}^0 = R_{jj^0}^c(N) + 2 \sum_{n=1}^N \sum_s \frac{V_{nj}^s V_{nj^0}^s}{E - \epsilon_n^s} ; \quad (\text{B 4})$$

A long similar lines, the vertex term, Eq. (30) is rewritten as

$$h_{jj}^f(\mathbf{E}) \delta_{ij}^0 = \sum_{n=1}^N \sum_s \frac{V_{nj}^s F_{nj^0}^s + F_{nj}^s V_{nj^0}^s}{E - \epsilon_n^s} + R_{jj^0}^f(N) ; \quad (\text{B 5})$$

with

$$R_{jj^0}^f(N) = \sum_{n=1}^N \sum_s \frac{V_{nj}^s F_{nj^0}^s + F_{nj}^s V_{nj^0}^s}{E - \epsilon_n^s} + \frac{1}{4} \int dr' \int dr \int dr^0 [V(\mathbf{r}; \mathbf{r}^0) f(\mathbf{r}^0; \mathbf{r}; 0) f(\mathbf{r}) + f(\mathbf{r}) f(\mathbf{r}; \mathbf{r}^0; 0) V(\mathbf{r}^0; \mathbf{r})] ; \quad (\text{B 6})$$

As an example, we have computed self-energy corrections in benzene including and not including the static remainder. With a static remainder, the first ionization energy decreases by 20 meV when N increases from 256 to 512, resulting in ionization potential of 9.30 eV for the larger value of N . Without static remainder, this ionization energy increases by 133 meV between the same choices of N , and its value for $N = 512$ is 8.27 eV, which is still far from convergence by as much as 1 eV.

In molecules and clusters, high-energy virtual states are expected to be very delocalized, and therefore sensitive to the choice of boundary conditions. In spite of that, the use of confined-system boundary conditions (where

all wave-functions are required to vanish outside some spherical enclosure) is still justified. The reason is that, as shown in Eq. (24), only the overlap between high-energy and low-energy states is relevant for self-energy calculations. The detailed features of high-energy states in the vacuum region, away from the atoms, are not very important. In addition, the contribution of virtual states in the summations over n decreases as one goes to higher and higher states. Nevertheless, the size of the confining region should always be tested against convergence, so that the shape of virtual states in the vicinity of atoms is correctly described.

- ¹ R.M. Martin, *Electronic Structure, Basic Theory and Practical Methods*, Cambridge Univ. Press, Cambridge, 2004; R.G. Parr and W. Yang, *Density-functional theory of atoms and molecules*, Oxford Univ. Press, Oxford (England), 1989; M.C. Payne, M.P. Teter, D.C. Allan, T.A. Arias, and J.D. Joannopoulos, *Rev. Mod. Phys.* 64, 1045 (1992).
- ² M.S. Hybertsen and S.G. Louie, *Phys. Rev. B* 34, 5390 (1986).
- ³ L. Hedin and S. Lundqvist, *Solid State Physics*, eds. F. Seitz, D. Turnbull, and H. Ehrenreich, vol. 23, 1, Academic, New York (1969).
- ⁴ W.G. Aulbur, L. Jonsson, and J.W. Wilkins, *Solid State Physics*, eds. F. Seitz, D. Turnbull, and H. Ehrenreich, vol. 54, 1, Academic, New York (2000).
- ⁵ A. Goring, H.H. Heinze, S.Ph. Ruzankin, M. Staufer, and N. Rosch, *J. Chem. Phys.* 110, 2785 (1999).
- ⁶ P. Rinke, A. Qteish, J. Neugebauer, C. Freysoldt, and M. Scheer, *New J. of Phys.* 7, 126 (2005); M. Stadelke, M. Mookara, J.A. Majewski, P. Vogl, and A. Goring, *Phys. Rev. B* 59, 10031 (1999).
- ⁷ G. Onida, L. Reining, and A. Rubio, *Rev. Mod. Phys.* 74, 601 (2002).

- ⁸ M. Rohlfing and S.G. Louie, *Phys. Rev. B* 62, 4927 (2000).
- ⁹ M. Rohlfing, *Int. J. of Quantum Chem.* 80, 807 (2000).
- ¹⁰ S. Albrecht, L. Reining, R. Del Sole, and G. Onida, *Phys. Rev. Lett.* 80, 4510 (1998); C.D. Spataru, S. Ismail-Beigi, L.X. Benedict, and S.G. Louie, *Phys. Rev. Lett.* 92, 077402 (2004); M. Rohlfing and S.G. Louie 82, 1959 (1999); E. Chang, G. Bussi, A. Ruini, and E. Molinari, *Phys. Rev. Lett.* 92, 196401 (2004); J.-W. van der Horst, P.A. Bobbert, M.A.J.M. Ichels, and H. Bassler, *J. Chem. Phys.* 114, 6950 (2001); P. Puschnig and C. Ambrosch-Daxl, *Phys. Rev. Lett.* 89, 056405 (2002).
- ¹¹ M.L. Tiago, J.E. Northrup, and S.G. Louie, *Phys. Rev. B* 67, 115212 (2003).
- ¹² J.C. Grossman, M. Rohlfing, L. Mitas, S.G. Louie, and M.L. Cohen, *Phys. Rev. Lett.* 86, 472 (2001).
- ¹³ H.-J. Eisler, V.C. Sundar, M.G. Bawendi, M. Walsh, H.J. Smith, and V.K. Limov, *Appl. Phys. Lett.* 80, 4614 (2002); K. Ichimura, S.K. Oh, and M. Nakagawa, *Science* 288, 1624 (2000).
- ¹⁴ V.N. Soloviev, A. Eichhofer, D. Fenske, and U. Banin, *J. Am. Chem. Soc.* 123, 2354 (2001); A.P. Alivisatos, *Science* 271, 933 (1996).
- ¹⁵ T.A. Niehaus, M. Rohlfing, F. Della Sala, A. Di Carlo, and

- Th. Frauenheim, *Phys. Rev. A* 71, 022508 (2005).
- ¹⁶ P.H. Hahn, W.G. Schmidt, and F. Bechstedt, *Phys. Rev. B* 72, 245425 (2005).
- ¹⁷ S. Ismail-Beigi and S.G. Louie, *Phys. Rev. Lett.* 90, 076401 (2003).
- ¹⁸ L.X. Benedict, A. Puzder, A.J. Williamson, J.C. Grossman, G.Galli, J.E. Klepeis, J.-Y. Raty, and O. Pankratov, *Phys. Rev. B* 68, 085310 (2003).
- ¹⁹ S. Ishii, K. Ohno, Y. Kawazoe, and S.G. Louie, *Phys. Rev. B* 63, 155104 (2001); S. Ishii, K. Ohno, Y. Kawazoe, and S.G. Louie, *Phys. Rev. B* 65, 245109 (2002).
- ²⁰ I. Vasiliev, S. Ogut, and J.R. Chelikowsky, *Phys. Rev. B* 65, 115416 (2002).
- ²¹ L. Reining, V. Olevano, A. Rubio, and G. Onida, *Phys. Rev. Lett.* 88, 066404 (2002).
- ²² R. Del Sole, O. Pulci, V. Olevano, and A. Marini, *Phys. Status Solidi B* 242, 2729 (2005); U. von Barth, N.E. Dahlén, R. van Leeuwen, and G. Stefanucci, *Phys. Rev. B* 72, 235109 (2005).
- ²³ A. Marini, R. Del Sole, and A. Rubio, *Phys. Rev. Lett.* 91, 256402 (2003); F. Sottile, V. Olevano, and L. Reining, *Phys. Rev. Lett.* 91, 056402 (2003); S. Botti, A. Fourreau, F. Nguyen, Y. O. Renault, F. Sottile, and L. Reining, *Phys. Rev. B* 72, 125203 (2005); S. Botti, F. Sottile, N. Vast, V. Olevano, L. Reining, H.C. Weissker, A. Rubio, G. Onida, R. Del Sole, and R.W. Godby, *Phys. Rev. B* 69, 155112 (2004); G. A. Dragna, R. Del Sole, and A. Marini, *Phys. Rev. B* 68, 165108 (2003).
- ²⁴ F. Bruneval, F. Sottile, V. Olevano, R. Del Sole, and L. Reining, *Phys. Rev. Lett.* 94, 186402 (2005).
- ²⁵ F. Sottile, F. Bruneval, A.G. Marinopoulos, L.K. Dash, S. Botti, V. Olevano, N. Vast, A. Rubio, and L. Reining, *Int. J. of Quantum Chem.* 102, 684 (2005).
- ²⁶ M.L. Tiago and J.R. Chelikowsky, *Solid State Commun.* 136, 333 (2005).
- ²⁷ E.K.J. Gross and W. Kohn, *Phys. Rev. Lett.* 55, 2850 (1985); *Adv. Quantum Chem.* 21, 255 (1990).
- ²⁸ M.E. Casida, in *Recent Advances in Density-Functional Methods, Part I*, ed. D.P. Chong (World Scientific, Singapore, 1995), p. 155.
- ²⁹ M.E. Casida, C. Jamorski, K.C. Casida, and D.R. Salahub, *J. Chem. Phys.* 108, 4439 (1998).
- ³⁰ C. Jamorski, M.E. Casida, and D.R. Salahub, *J. Chem. Phys.* 104, 5134 (1996).
- ³¹ G. Strinati, *Riv. Nuovo Cimento* 11, 1 (1988).
- ³² W. Kohn and L.J. Sham, *Phys. Rev.* 140, A1133 (1965).
- ³³ S.L. Adler, *Phys. Rev.* 126, 413 (1962); N.W.iser, *Phys. Rev.* 129, 62 (1963).
- ³⁴ S. Ogut, R. Burdick, Y. Saad, and J.R. Chelikowsky, *Phys. Rev. Lett.* 90, 127401 (2003).
- ³⁵ R.W. Godby, M. Schlüter, and L.J. Sham, *Phys. Rev. B* 37, 10159 (1988).
- ³⁶ E.L. Shirley and R.M. Martin, *Phys. Rev. B* 47, 15404 (1993); E.L. Shirley and R.M. Martin, *Phys. Rev. B* 47, 15413 (1993).
- ³⁷ L. Hedin, *Int. J. Quantum Chem.* 56, 445 (1995).
- ³⁸ R. Del Sole, L. Reining, and R.W. Godby, *Phys. Rev. B* 49, 8024 (1994).
- ³⁹ A. Fleszar and W. Hanke, *Phys. Rev. B* 71, 045207 (2005); S.V. Faleev, M. van Schilfgaarde, and T. Kotani, *Phys. Rev. Lett.* 93, 126406 (2004); W. Ku and A.G. Eguiluz, *Phys. Rev. Lett.* 89, 126401 (2002); W. Ku and A.G. Eguiluz, *Phys. Rev. Lett.* 93, 249702 (2004); K. Delaney, P. Garcia-Gonzalez, A. Rubio, P. Rinke, and R.W. Godby, *Phys. Rev. Lett.* 93, 249701 (2004); M.L. Tiago, S. Ismail-Beigi, and S.G. Louie, *Phys. Rev. B* 69, 125212 (2004); R.T.M. Ummels, P.A. Bobbert, and W. van Haeringen, *Phys. Rev. B* 57, 11962 (1998).
- ⁴⁰ D.F. DuBois, *Ann. Phys.* 7, 174 (1959); *Ann. Phys.* 8, 24 (1959).
- ⁴¹ B. Holm and U. von Barth, *Phys. Rev. B* 57, 2108 (1998); U. von Barth and B. Holm, *Phys. Rev. B* 54, 8411 (1996); *Phys. Rev. B* 55, 10120 (1997).
- ⁴² F. Furche, *J. Chem. Phys.* 114, 5982 (2001); B. Walker, A.M. Saitta, R. Gebauer, and S. Baroni, *Phys. Rev. Lett.* 96, 113001 (2006).
- ⁴³ J.P. Perdew and A. Zunger, *Phys. Rev. B* 23, 5048 (1981); D.M. Ceperley and B.J. Alder, *Phys. Rev. Lett.* 45, 566 (1980).
- ⁴⁴ N. Troullier and J.L. Martins, *Phys. Rev. B* 43, 1993 (1990).
- ⁴⁵ J.R. Chelikowsky, N. Troullier, and Y. Saad, *Phys. Rev. Lett.* 72, 1240 (1994); J.R. Chelikowsky, N. Troullier, K. Wu, and Y. Saad, *Phys. Rev. B* 50, 11355 (1994).
- ⁴⁶ NIST Chemistry Webbook, NIST Standard Reference Database Number 69, edited by P.J. Linstrom and W.G. Mallard (National Institute of Standards and Technology, Gaithersburg, MD, 2001) (<http://webbook.nist.gov>).
- ⁴⁷ G.F. Bertsch, A. Schnell, and K. Yabana, *J. Chem. Phys.* 115, 4051 (2001).
- ⁴⁸ S.P. Park, S.S. Kim, J.H. Kim, C.N. Whang, and S. Im, *Appl. Phys. Lett.* 80, 2872 (2002).
- ⁴⁹ J.B. Krieger, Y. Li, G.J. Taffate, *Phys. Rev. A* 45, 101 (1992).
- ⁵⁰ J.F. Janak, *Phys. Rev. B* 18, 7165 (1978).
- ⁵¹ C.-G. Zhan, J.A. Nichols, and D.A. Dixon, *J. Phys. Chem. A* 107, 4184 (2003).
- ⁵² F. Della Sala and A. Gorling, *J. Chem. Phys.* 115, 5718 (2001).
- ⁵³ A. Gorling, *Phys. Rev. Lett.* 83, 5459 (1999).
- ⁵⁴ N.O. Lipari, C.B. Duke, and L. Pietronero, *J. Chem. Phys.* 65, 1165 (1976).
- ⁵⁵ M.S. Deluze, L. Claes, E.S. Kryachko, and J.-P. Francois, *J. Chem. Phys.* 119, 3106 (2003).
- ⁵⁶ S. Hirata, C.-G. Zhan, E. Apra, T.L. Windus, and D.A. Dixon, *J. Phys. Chem. A* 107, 10154 (2003).
- ⁵⁷ J.C. Rienstra-Kiracofe, C.J. Barden, S.T. Brown, and H.F. Schaefer III, *J. Phys. Chem. A* 105, 524 (2001).
- ⁵⁸ P.D. Burrow, J.A. Michels, and K.D. Jordan, *J. Chem. Phys.* 86, 9 (1987).
- ⁵⁹ I. Vasiliev and R.M. Martin, *Phys. Rev. A* 69, 052508 (2004).
- ⁶⁰ G. Herzberg, *Molecular Spectra and Molecular Structure*, vol. III, *Electronic Spectra and Electronic Structure of Polyatomic Molecules*, Van Nostrand, New York, 1966.
- ⁶¹ E.E. Koch and A. Otto, *Chem. Phys. Lett.* 12, 476 (1976).
- ⁶² J. Lorentzon, P. Malmquist, M. Fulscher, and B.O. Roos, *Theor. Chim. Acta* 91, 91 (1995).
- ⁶³ H.H. Heinze, A. Gorling, and N. Rosch, *J. Chem. Phys.* 113, 2088 (2000).
- ⁶⁴ J.P. Doring, *J. Chem. Phys.* 51, 2866 (1969).
- ⁶⁵ M. Rubio, M. Merchán, E. Orti, and B.O. Roos, *Chem. Phys.* 179, 395 (1993).
- ⁶⁶ G.A. George and G.C. Morris, *J. Mol. Spectrosc.* 26, 67 (1968).
- ⁶⁷ M.J.S. Dewar and S.D. Worley, *J. Chem. Phys.* 50, 654 (1969).

- ⁶⁸ B.C. Lin, C.P. Cheng, and Z.P.M. Lao, *J. Phys. Chem. A* 107, 5241 (2003).
- ⁶⁹ T. Heinis, S. Chowdhury, and P. K. Ebarle, *Org. Mass Spectrom.* 28, 358 (1993).
- ⁷⁰ A. Zlatkis, C.K. Lee, and W.E. Wentworth, *Anal. Chem.* 55, 1596 (1983).
- ⁷¹ U. Itoh, Y. Toyoshima, and H. Onuki, *J. Chem. Phys.* 85, 4867 (1986).
- ⁷² L. Mitas, J. Therrien, R. Twisten, G. Belomoin, and M.H. Nayfeh, *Appl. Phys. Lett.* 78, 1918 (2001).
- ⁷³ Y.-H. Kim and A. Gorling, *Phys. Rev. Lett.* 89, 096402 (2002).
- ⁷⁴ L.E. Brus, *J. Chem. Phys.* 79, 5566 (1983); *ibid.* 80, 4403 (1984).
- ⁷⁵ L.A. Cole and J.P. Perdew, *Phys. Rev. A* 25, 1265 (1982).
- ⁷⁶ M. Rohling and S.G. Louie, *Phys. Rev. Lett.* 80, 3320 (1998).
- ⁷⁷ V. Olevano and L. Reining, *Phys. Rev. Lett.* 86, 5962 (2001).
- ⁷⁸ M. Born and E. Wolf, *Principles of Optics: electromagnetic theory of propagation, interference and diffraction of light*, 7th Ed., Section 14.5, Cambridge University Press, Cambridge (UK), 1999; J.C. Maxwell-Garnett, *Philos. Trans. Royal Soc. London* 203A, 385 (1904).
- ⁷⁹ A. Tsolakidis and R.M. Martin, *Phys. Rev. B* 71, 125319 (2005).
- ⁸⁰ X. Zhao, C.M. Wei, L. Yang, and M.Y. Chou, *Phys. Rev. Lett.* 92, 236805 (2004); F. Bruneval, S. Botti, and L. Reining, *Phys. Rev. Lett.* 94, 219701 (2005); X. Zhao, C.M. Wei, L. Yang, and M.Y. Chou, *Phys. Rev. Lett.* 94, 219702 (2005).
- ⁸¹ W. Hanke, *Adv. Phys.* 27, 287 (1978).
- ⁸² B. Delley and E.F. Steigmeyer, *Phys. Rev. B* 47, 1397 (1993).
- ⁸³ A.J. Williamson, J.C. Grossman, R.Q. Hood, A. Puzder, and G. Galli, *Phys. Rev. Lett.* 89, 196803 (2002).
- ⁸⁴ M.M.G. Alemany, M. Jain, L. Kronik, and J.R. CheLIKowsky, *Phys. Rev. B* 69, 075101 (2004).
- ⁸⁵ G. Baldini and B. Bosacchi, *Phys. Status Solidi* 38, 325 (1970).
- ⁸⁶ M.P. Sumr, H. Chacham, and S.G. Louie, *Phys. Rev. B* 51, 7464 (1995).
- ⁸⁷ C.J. Buchenauer and D.B. Fitch, *Phys. Rev.* 167, 846 (1968).
- ⁸⁸ K. Takiyama, *J. Phys. Soc. Jpn.* 44, 1627 (1978).
- ⁸⁹ C.C. Klink, *Phys. Rev.* 137, A1814 (1965).
- ⁹⁰ F.C. Brown, Ch. Gahwiler, H. Fujita, A.B. Kunz, W. Scheiety, and N. Carrera, *Phys. Rev. B* 2, 2126 (1970).
- ⁹¹ L.A. Curtiss, P.C. Redfern, K. Raghavachari, and J.A. Pople, *J. Chem. Phys.* 109, 42 (2003); L.A. Curtiss, K. Raghavachari, P.C. Redfern, V. Rassolov, and J.A. Pople, *J. Chem. Phys.* 109, 7764 (2003).
- ⁹² L. Reining, G. Onida, and R.W. Godby, *Phys. Rev. B* 56, R4301 (1997).
- ⁹³ As written, Eq. (2) corresponds to a time-ordered function, but it differs from the causal (measurable) response function only for negative values of energy.
- ⁹⁴ Comparing earlier work⁸, we have observed that the Tamm-Danco approximation (i.e., neglecting mixing between absorption and emission contributions) is acceptable when calculating excitation energies in the GW + BSE framework. This contrasts with the scenario in TDDFT, where mixing is usually important^{7,28,42}, due to the specific properties of the TDDFT kernels. The impact of the Tamm-Danco approximation in the energy loss spectrum of silicon has been analyzed by Olevano and Reining⁷⁷.
- ⁹⁵ The value of 7.4 eV reported in Ref.²⁰ for the peak position has been recently revised to 7.1 eV in Ref.⁵⁹.
- ⁹⁶ The inaccurate optical gap reflects the gap underestimation inherent to DFT, and it can be corrected by an ad hoc scissors operator. The lack of excitonic effects should be attributed to the specific functional employed in TD-LDA, since other functionals were shown to correctly predict the enhancement of the E_1 peak relative to E_2 ^{21,73}.